Short-term exposure to intermittent hypoxia leads to changes in gene expression seen in chronic pulmonary disease

Gang Wu[1]*, Yin Yeng Lee[1,2]*, Evelyn M. Gulla[3], Andrew Potter[4], Joseph Kitzmiller[5], Marc D Ruben[1], Nathan Salomonis[2,6], Jeffrey A. Whitsett[5], Lauren J Francey[1], John B Hogenesch[1], David F. Smith[3,7,8,9]
*Both authors contributed equally.

[1] Divisions of Human Genetics and Immunobiology, Center for Chronobiology, Department of Pediatrics, Cincinnati Children's Hospital Medical Center, Cincinnati, OH 45229, USA

[2] Department of Pharmacology and Systems Physiology, University of Cincinnati College of Medicine, Cincinnati, OH 45229, USA

[3] Division of Pediatric Otolaryngology-Head and Neck Surgery, Cincinnati Children's Hospital Medical Center, Cincinnati, OH 45229, USA

[4] Division of Developmental Biology, Cincinnati Children's Hospital Medical Center, Cincinnati, OH 45229, USA

[5] Division of Pulmonary Biology, Cincinnati Children's Hospital Medical Center, Cincinnati, OH 45229, USA

[6] Division of Biomedical Informatics, Cincinnati Children's Hospital Medical Center, Cincinnati, OH 45229, USA

[7] Division of Pulmonary Medicine, Cincinnati Children's Hospital Medical Center, Cincinnati, OH 45229, USA

[8] The Sleep Center, Cincinnati Children's Hospital Medical Center, Cincinnati, OH 45229, USA

[9] Department of Otolaryngology-Head and Neck Surgery, University of Cincinnati College of Medicine, Cincinnati, OH 45267, USA

Corresponding Author:

David F Smith, MD, PhD
Assistant Professor
Divisions of Pediatric Otolaryngology, Pulmonary Medicine, and the Sleep Center
Cincinnati Children's Hospital Medical Center
Department of Otolaryngology-Head and Neck Surgery
University of Cincinnati School of Medicine
Cincinnati, OH 45229
Phone: (513) 803-4194
Fax: (513) 636-8133
Email: David.Smith3@cchmc.org

Keywords: obstructive sleep apnea, single cell sequencing, intermittent hypoxia, lung, RNA sequencing

Abstract

Obstructive sleep apnea (OSA) results from episodes of airway collapse and intermittent hypoxia and is associated with a host of health complications including dementia, diabetes, heart failure, and stroke. Although the lung is the first organ to sense changes in inspired oxygen levels, little is known about the consequences of IH to the lung hypoxia-inducible factor (HIF)-responsive pathways. Furthermore, cellular mechanisms causing disease progression across multiple systems in OSA are unknown. We hypothesized that exposure to IH would lead to up- and down-regulation of diverse expression pathways and that individual cell populations would show distinctive responses to IH. We identify changes in circadian and immune pathways in lungs from mice exposed to IH. Among all cell types, endothelial cells show the most prominent transcriptional changes. Interestingly, up-regulated genes in endothelial, fibroblast, and myofibroblast cells were enriched for genes associated with pulmonary fibrosis and pulmonary hypertension. These genes include targets of several drugs currently used to treat chronic pulmonary diseases. Our results reveal potential candidates for cell-targeted therapy seeking to minimize pulmonary effects of OSA. A better understanding of the pathophysiologic mechanisms underlying diseases associated with OSA could improve our therapeutic approaches, directing therapies to the most relevant cells and molecular pathways.

Introduction

Obstructive sleep apnea (OSA) is a condition characterized by episodes of sleep-associated upper airway obstruction and intermittent hypoxia (IH). OSA occurs in approximately 2-5% of children(Marcus et al., 2012) and 33% of adults 30-69 years of age(Benjafield et al., 2019) in the US. If untreated, OSA is associated with significant health consequences to the cardiovascular, neurological, and metabolic systems. Even young children with moderate to severe OSA can develop blood pressure dysregulation(Amin et al., 2004), systemic hypertension(Enright et al., 2003; Kohyama et al., 2003), and left ventricular hypertrophy(Amin

68 et al., 2002, 2005). OSA is associated with a significant socioeconomic burden in the
69 US(Sullivan, 2016). Despite available medical and surgical therapies, millions of children and
70 adults with OSA are currently untreated or do not respond to available therapies. Cellular
71 responses to changes in oxygen levels are primarily mediated by the hypoxia-inducible factors
72 (HIFs). Although the lung is the first organ to sense large changes in inspired oxygen levels,
73 little is known about the consequences of IH to the lung HIF-responsive pathways. Without a
74 basic understanding of the molecular mechanisms that lead to diseases associated with IH and
75 OSA, our ability to identify new treatments is significantly hindered.

76 Efforts to understand the effects of OSA have primarily focused on systemic
77 inflammation(Gozal et al., 2008), oxidative stress(Tauman et al., 2014), and endothelial
78 dysfunction(Bhattacharjee et al., 2012; Kheirandish-Gozal et al., 2013). However, the early
79 causal events from IH-exposure are not fully elucidated. Research is now focused on other
80 possible pathogenic pathways that could be activated or suppressed in the presence of IH,
81 leading to disease. For example, hypoxia inducible factors (HIFs) stabilized under low oxygen
82 conditions can affect the circadian transcriptional-translational feedback loop at the cellular
83 level(Adamovich et al., 2017; Hogenesch et al., 1998; Kobayashi et al., 2017; Peek et al., 2017;
84 Wu et al., 2017). Even acute exposure to IH results in dysregulation of the circadian clock that is
85 time-of-day-dependent and tissue-specific, and these effects persist in some tissue for up to 24
86 hours after exposure(Manella et al., 2020). Pathways involved in immune responses and
87 regulation can also be activated or suppressed in the presence of IH(Cubillos-Zapata et al.,
88 2017; Lam & Ip, 2019), contributing to comorbid disease initiation and progression. Associations
89 between IH and gene targets could be either pathogenic or protective responses for the lung.
90 Additionally, lung could be an effector rather than target organ of IH, resulting in responses to IH
91 that lead to multi-systemic effects.

While animal models of OSA have focused on physiologic responses to IH at organ and system levels, determination of the contributions of individual cell types in initiation and progression of disease has been challenging. Within organs, individual cells serve specific physiologic roles. As a result, pathways disrupted by stabilization of HIFs can affect cell types differently. Single-cell RNA sequencing (scRNA-seq) has emerged as a method for evaluating transcriptional states from thousands of individual cells(M. J. Zhang et al., 2018), advancing our understanding of how specific cell types contribute to physiology and disease(Plasschaert et al., 2018; M. J. Zhang et al., 2018).

In the present study, we used IH as a mouse model of OSA to better understand early cellular-specific consequences to the lung, the primary organ that first senses hypoxic episodes. We hypothesized that exposure to IH would lead to up- and down-regulation of diverse expression pathways, distinct cell populations would show distinctive responses to IH, and that changes in these gene expression pathways could provide therapeutic targets at the cell-specific level. We identify changes in both circadian and immune response pathways in lungs from mice exposed to IH. We also demonstrate strong similarities in the gene expression profiles from mice compared to those characteristics of human lung tissue from patients with diverse pulmonary diseases, including pulmonary hypertension and pulmonary fibrosis. Our results reveal potential candidates for cell-targeted therapy seeking to minimize effector responses of the lung that could lend to systemic disease. A better understanding of the pathophysiologic mechanisms underlying diseases associated with OSA could improve our therapeutic approaches.

Results

Short-term exposure to intermittent hypoxia reshapes circadian and immune pathways in the lung

116 In humans, moderate to severe OSA is associated with interstitial lung disease with remodeling
117 of the extracellular matrix(Kim et al., 2017). Lung is the primary organ that senses episodes of
118 hypoxia and is therefore exposed to large fluctuations in the oxygen concentrations compared to
119 other tissues throughout the body. For these reasons, we sought to identify initial changes in
120 gene expression pathways in the lung in response to IH.

121 Mice were initially entrained to the same light:dark schedule to synchronize active and
122 inactive phases. After 14 days of entrainment in the 12h:12h light:dark cycle, mice were
123 exposed to IH or room air (normoxia) for the entire 12h inactive phase for 9 days (Fig. 1A). Mice
124 tolerated the procedure well. Furthermore, haemotoxylin and eosin (H&E) staining of whole
125 lungs did not show gross changes in architecture or inflammatory remodeling after exposure to
126 IH (Fig. S1). Bulk RNA-seq was performed to explore transcriptomic effects of IH on lung tissue
127 at the organ level. There were 374 genes (Fig. S2A) up-regulated and 149 down-regulated in
128 mouse lung after exposure to IH (BHQ < 0.05 and fold change >1.5). Not surprisingly, the top
129 up-regulated genes included well-known hypoxia inducible factor (HIF)-1 target genes (e.g.
130 *Edn1*, *Bnip3* and *Ankrd37*; Fig. S2B).

131 We performed DAVID(Huang et al., 2009) enrichment analysis to identify biological
132 processes associated with the top 200 up and down regulated genes from mice exposed to IH.
133 Pathways induced in response to hypoxia included circadian rhythm, angiogenesis, and
134 extracellular matrix organization (Fig. 1B and C). Increased expression of RNAs associated with
135 angiogenesis, such as vascular endothelial growth factor (VEGF), was observed after IH,
136 consistent with findings in a mouse model of prolonged exposure to IH(Reinke et al., 2011) and
137 after 72 h of IH exposure to endothelial cells *in vitro(Wohlrab et al., 2018)*. Unexpectedly, RNAs
138 associated with immune responses were significantly down regulated after 9 days of IH (Fig. 1B
139 and C). Present findings contrast with the general concept that HIFs are important regulators of
140 inflammation and immune responses (Eltzschig & Carmeliet, 2011; Scholz & Taylor, 2013; C. T.

141 Taylor et al., 2016). For example, activation of neutrophils by HIFs is largely considered
142 proinflammatory(Peyssonnaux et al., 2005; C. T. Taylor et al., 2016; Walmsley et al., 2005). As
143 previously reported, there is a tight interaction between clock genes and HIFs(Edgar et al.,
144 2012; Gu et al., 2000; Hogenesch et al., 1998; McIntosh et al., 2010; B. L. Taylor & Zhulin,
145 1999). Several circadian clock repressors (e.g. *Nr1d1*, *Nr1d2*, *Bhlhe40* and *Per3*) were
146 significantly upregulated in the IH group (Fig. 1C).

147 **Single cell sequencing identifies 19 distinct cell types in the lungs of intermittent hypoxia**
148 **and control mice**

149 We detected significant differences related to a number of cell-type selective genes on
150 biological functions. We then applied single cell transcriptomics to identify cell-type specific
151 effects of IH. In total, we sequenced 12,324 and 16,125 pulmonary cells from IH and control
152 mice. Unsupervised analysis identified 25 transcriptionally distinct cell clusters, corresponding to
153 19 distinct cell types (Fig. 2A-C) based on the expression of established marker genes (See
154 Methods), including stromal, epithelial, endothelial, immune, as well as small numbers of other
155 cell types. The proportion of endothelial, AT2, fibroblast/myofibroblast cells were modestly
156 increased, but the proportion of immune cells (e.g. B and T cells) was decreased in the IH
157 exposed mice (Fig. 2C). Overall, the variation of lung cell types was small (BHQ > 0.05). Given
158 that this was a short exposure of IH, we did not anticipate a dramatic difference in cell types or
159 proportions. We then examined samples to determine if lungs from control vs experimental mice
160 showed histologic differences in cell types.

161 **Short-term exposure to intermittent hypoxia did not lead to histologic changes in the**
162 **lung**

163 Similar to H&E histology, confocal immunofluorescence microscopy for major cell types were
164 normal without inflammatory remodeling. Immunostaining for endothelial markers LYVE1 and
165 FOXF1 did not show changes in IH exposed mice (Fig. 3C-D) compared to normoxia (Fig. 3A-

166 B). Also important, staining for MKI67 did not show changes in endothelial cell proliferation (Fig.
167 3E-H). Expression levels of HOPX and SFTPC in alveolar type I and type II cells were not
168 significantly different for IH (Fig. 3K-L) versus control (Fig. 3I-J) mice. Immunostaining for the
169 progenitor marker SOX9 (Fig. 3I-L) or the extracellular matrix marker POSTN (Fig. 3M-P) did
170 not demonstrate any changes after IH exposure. Overall, there were no differences in
171 endothelial or epithelial cells, signs of fibrosis, or increases in the number of progenitor or
172 proliferating cells. Although other studies have demonstrated changes in proliferating type II
173 alveolocytes(Reinke et al., 2011) and pulmonary vascular remodeling(Nisbet et al., 2009), these
174 were chronic mouse models of IH involving months of exposure. These models also produced
175 other phenotypic changes, such as increased lung volumes(Reinke et al., 2011) and pulmonary
176 hypertension(Nisbet et al., 2009). We exposed our mice to IH for a shorter period of time to
177 specifically evaluate the changes in gene expression prior to lung remodeling with the hope of
178 uncovering early pathways that lead to disease.

179 **Diverse expression pathways were up and down regulated in the presence of intermittent**
180 **hypoxia**

181 We further explored the early cell-type specific response to IH in mouse lung by aggregating
182 single cell data into “pseudo-bulk” data to compare biological replicates for each identified cell
183 type (see Methods for details). Using DESeq2(Love et al., 2014), the number of up or down
184 regulated genes in different lung cell types in response to IH are not equal (Fig. S3). To balance
185 the difference in the pathway enrichment analysis, we selected the top 200 up and down
186 regulated genes (ranking by the *P* value) in each cell type. From the DAVID enrichment
187 analysis, diverse biological processes were up and down regulated in different cell types in
188 response to IH (Fig. 4A, Fig. S4 A and B). For example, hypoxia-responsive and circadian
189 pathways were enriched in those up regulated genes in response to IH in endothelial cells,
190 myofibroblasts, and AT2 cells. Immune response-related and antigen processing and

191 presentation were enriched in those down regulated genes in monocytes, macrophages-
192 dendritic cells, NK cells, and erythroblasts. Surprisingly, circadian pathways were highly
193 enriched in multiple cell populations, not just epithelial cells, a population that is important for
194 circadian rhythmicity in the lung(Gibbs et al., 2009). As expected from specific genes in each
195 biological process, the response level of the same genes were different in multiple cell types
196 (Fig. 4B and C). For example, the circadian repressor gene, *Nr1d1,* was more responsive to IH
197 in endothelial and AT2 cells than lymphatic endothelial cells and AT1 cells. We also noted cell-
198 specific responses for the down regulated genes. For example, immune response genes (e.g.
199 *Iglc3*, *S100a8*, and *Oas3*) decreased more in monocytes than macrophages in response to IH.

200 **Pulmonary vascular endothelial subpopulations show distinctive responses to**
201 **intermittent hypoxia**

202 Recent studies show distinct vascular endothelial cell subpopulations in mouse and human
203 lung(Ren et al., 2019). Our vascular endothelial populations were annotated to endothelial
204 artery, vein, capillary aerocytes (Cap-a), and general capillary (Cap-g) cells (Fig. 5A and Fig.
205 S5). Interestingly, we found that endothelial cells demonstrated profound changes in gene
206 expression profiles in response to IH. The endothelial capillary cells were more responsive to IH
207 compared to endothelial artery and vein cells (Fig. 5B). For example, at BHQ < 0.2, more than
208 100 genes were significantly up-regulated in capillary aerocytes and general capillary cells.
209 However, only 1 gene in the arterial endothelial cells and 57 genes in the venular endothelial
210 cells were significantly up-regulated at the same cutoff. This trend persisted at other BHQ cut-
211 offs (Fig. S6). General capillary cells are more responsive to hypoxia than capillary aerocytes. In
212 addition, more genes were significantly up and down regulated in general capillary cells (Fig.
213 5B). Hypoxia-responsive genes (e.g. *Pdk1*, *Vegfc*, *Slc2a1*, *Pkm*, and *Flt1*) showed higher levels
214 of expression variation (fold change and significance) in general capillary cells than capillary
215 aerocytes (Fig. 5C), demonstrating variation at the subpopulation level. Glycolytic process was

216 up regulated and cell migration was down regulated in both capillary aerocytes and general
217 capillary cells in response to IH (Fig. 5D and E). Given the association between glycolysis,
218 cytoskeletal remodeling, and cell migration in other cell types(Shiraishi et al., 2015), the similar
219 enrichment trends for these pathways is not surprising. Additionally, without vascular growth
220 associated with chronic IH, glycolysis may be used to meet metabolic demand. Interestingly,
221 changes in the glycolytic process were specific to endothelial cell types (Fig. S4B).

222 On the other hand, capillary aerocytes and general capillary cells demonstrated more
223 differences in enrichment pathways (Fig. 5D and E). For example, circadian rhythm and
224 regulation of angiogenesis were only enriched for those up and down regulated genes in
225 general capillary cells in response to IH, while phagocytosis and regulation of cell shape were
226 only enriched for those down regulated genes in capillary aerocytes (Fig. 5D and E, table S12).
227 Anatomic location within the pulmonary vasculature, including variable roles in gas exchange,
228 could lead to these differences in response. Alternatively, proximity and interaction with other
229 cell types, such as fibroblasts or immune cells, could also help to explain these findings.

230 Evaluation of the expression pathways at the single cell resolution demonstrated
231 significant changes in multiple cell types. With this information, we wanted to identify potential
232 candidates for therapeutic intervention in response to IH.

233 **Pulmonary disease-regulated genes provide clinical implications for OSA at the cell-**
234 **specific level**

235 OSA is associated with an array of pulmonary diseases, such as interstitial lung disease (Kim et
236 al., 2017), idiopathic pulmonary fibrosis (Lancaster et al., 2009), and pulmonary hypertension
237 (Chaouat et al., 1996; Dimitar Sajkov & McEvoy, 2009). IH led to significantly more up than
238 down regulated genes (Fig. 6A and Fig. S7). IH-induced expression in myofibroblasts,
239 fibroblasts, AT2 cells, basophils, and macrophage-DCs were significantly enriched for chronic
240 obstructive pulmonary disease (COPD)-associated genes, while myofibroblasts and fibroblasts

241 demonstrated enrichment of genes associated with pulmonary fibrosis. However, the disease
242 genes were not equally expressed or up regulated in these cell types (Fig. 6B). For example,
243 *Ptgis* is a pulmonary hypertension-associated gene highly expressed in myofibroblasts and
244 fibroblasts compared to other cell types (Fig. S8). *Ptgis* is also a target gene for Epoprostenol—
245 a drug used for treating pulmonary hypertension(Sitbon & Vonk Noordegraaf, 2017). The
246 idiopathic pulmonary fibrosis-associated gene, *Thbs1(Idell et al., 1989; Kuhn & Mason, 1995;*
247 *Yehualaeshet et al., 2000)*, was highly expressed and more responsive to IH in myofibroblasts
248 compared to other cell types. *Msr1(Hersh et al., 2006; Silverman et al., 2002)* is a COPD-
249 associated gene which was highly expressed in macrophage-DCs, basophils, and monocytes.
250 These data highlight the similarity of the IH signatures with cell-type specific responses in an
251 array of pulmonary diseases (Fig. 6C, Fig. S8).

252 We further evaluated changes in the interactions of these drug-targeted disease genes
253 in each cell type using CellPhoneDB(Vento-Tormo et al., 2018). There are 32 ligand-receptor
254 interactions found in the database using these drug-targeted disease genes. Overall,
255 myofibroblasts were involved in 98 out of 176 gains of interaction (BHQ=4.28e-50),
256 demonstrating the significance of this cell type in activating the FGF signaling pathway in early
257 IH-associated responses (Fig. 6D, Fig. S9).

258 **Discussion**

259 OSA results from intermittent episodes of airway collapse and hypoxemia and is associated with
260 dementia(Osorio et al., 2015), diabetes(Punjabi & Beamer, 2009), hypertension(Marin et al.,
261 2012), heart failure(Gottlieb et al., 2010), and stroke(Valham et al., 2008). How cellular
262 responses to hypoxia and hypoxemia initiate and cause disease progression in multiple organs
263 remains unknown. Using IH as a mouse model of OSA, we show profound, cell-type specific
264 changes in genome-wide RNA expression in the lung. RNA profiles from lungs of mice exposed
265 to IH shared similarity with gene expression changes in human lung from patients with

266 pulmonary disease, including pulmonary hypertension, COPD, and asthma. OSA is associated
267 with injury to alveolar epithelial cells and extracellular matrix remodeling, key features of
268 interstitial lung disease (Kim et al., 2017). Although it is known that pulmonary diseases share
269 general mechanisms, such as systemic inflammation and oxidative stress(McNicholas, 2009),
270 there is an incomplete understanding of the early-stage changes in the lung from OSA.

271 In the present study, macrophages, dendritic cells, and NK cells were the only
272 populations to demonstrate altered oxidation-reduction in the early stages of IH exposure. It was
273 previously demonstrated that chronic IH in mice caused the release of free oxygen radicals in
274 the lung(Tuleta et al., 2016), effects that could be blunted with antioxidative agents(Tuleta et al.,
275 2016). Pulmonary hypertension from chronic IH was associated with enhanced NADPH oxidase
276 expression, and knockout mice lacking one of these subunits demonstrated attenuated effects
277 of chronic IH(Nisbet et al., 2009). Which cells mediate these effects in the lung? This type of
278 knowledge can help direct therapeutics to the most relevant cells and molecular pathways.

279 In our mice exposed to IH, prostacyclin synthase (*Ptgis*) expression was dramatically
280 upregulated in myofibroblasts and fibroblasts, and to a lesser degree macrophages. As a potent
281 vasodilator and inhibitor of platelet aggregation, therapies targeting this pathway are already
282 used for patients with pulmonary arterial hypertension(Farber & Gin-Sing, 2016). Given the
283 association between OSA and pulmonary hypertension(Bady et al., 2000; D. Sajkov et al.,
284 1999), further work can determine the clinical potential from targeting these pathways. As
285 another example, IH downregulated fibroblast growth factor receptor (FGFR-2) in alveolar type
286 2 cells. FGFR2 promotes alveolar regeneration in response to lung injury(Perl & Gale, 2009),
287 and is upregulated in patients with idiopathic pulmonary fibrosis(Li et al., 2018). Previous
288 studies suggest that OSA can induce injury to the lung(Aihara et al., 2011; Lederer et al., 2009),
289 and OSA is prevalent in patients with idiopathic pulmonary fibrosis(Lancaster et al., 2009). If

290 OSA does, in fact, lead to fibrotic changes in the lung, targeting FGF pathways in alveolar
291 epithelial cells could prevent disease progression from IH.

292 Although there is limited data on the role of the circadian clock in OSA(von Allmen et al.,
293 2018), it may play a significant role in this disease(Butler et al., 2015; Entzian et al., 1996; Smith
294 et al., 2017). We found dysregulation of circadian gene expression in multiple cell types. The
295 circadian clock is a transcriptional/translational feedback loop that coordinates 24 h timing of
296 physiological functions. BMAL1, the key clock transcription factor(Hogenesch et al., 1998),
297 interacts with CLOCK(King et al., 1997) and it's partner NPAS2(Zhou et al., 1997) to activate
298 hundreds of target genes. All three are members of the basic helix-loop-helix (bHLH)-PER-
299 ARNT-SIM (PAS) transcription factor family. The HIFs (1-3) are members of the same
300 transcription factor family and are stabilized under low oxygen conditions. It is known that the
301 circadian clock in alveolar epithelial cells impacts pulmonary physiology, and it's disruption can
302 contribute to disease in animal models(Z. Zhang et al., 2019). More importantly, IH leads to
303 intertissue circadian misalignment (including in the lung) in mice(Manella et al., 2020). The
304 hypoxic episodes that define OSA are clearly diurnal, but we don't understand if clock disruption
305 is a cause or consequence of disease. Our findings suggest that circadian clock dysfunction
306 may be an important early-stage consequence of hypoxia-driven disease and may contribute to
307 downstream processes.

308 Lung samples from IH-exposed mice did *not* show comprehensive histopathologic
309 changes. This contrasts with findings from some prior murine models of IH. For example, IH
310 induced epithelial cell proliferation in lungs from a chronic exposure model (Reinke et al., 2011).
311 In a bleomycin-induced lung injury model, fibrosis in mouse lung is worsened by IH(Gille et al.,
312 2018). In our model, short-term exposure to IH did not result in changes to the parenchyma or
313 vessels. This is likely attributed to the difference in the length of time of IH exposure. Future
314 longitudinal studies should address how gene expression profiles change over time and which

315 cell types drive disease progression from early to late IH exposure. Early insults from hypoxia
316 may also drive organ-specific damage in other systems. Although models of IH replicate
317 desaturation and recovery of fractional inhaled oxygen, there is variability in the number of
318 hypoxic events, length of desaturation events, and length of overall exposure. This variability
319 could affect expression profiles and histopathologic findings.

320 Our data provide insight into the early cellular responses that drive disease progression
321 in OSA. By identifying the roles of individual cells in disease, we have the opportunity to test
322 targeted therapeutics, focusing specifically on the most pathologically-relevant cells and
323 molecular pathways. Studies using scRNA-seq are already being used to identify novel cell
324 populations in disease. For example, Xu and colleagues(Xu et al., 2016) identified a loss of
325 normal epithelial cells in the development of idiopathic pulmonary fibrosis. In another study
326 using single-cell profiling of bronchial epithelial cells, the major source of cystic fibrosis
327 transmembrane conductance regulator (CFTR) activity, the pulmonary ionocyte, was
328 revealed(Plasschaert et al., 2018). As *CFTR* is the gene mutated in cystic fibrosis, cell-specific
329 therapies for this disease can now be evaluated.

330 Delineating the upstream processes dysregulated in OSA could help us identify potential
331 candidates for therapeutic intervention. Given the socioeconomic burden to our healthcare
332 system for diagnosing and treating OSA, new diagnostic and therapeutic strategies will be vital
333 for the coming years.

334 **Materials and Methods**

335 *Animals*. Use of animals and all procedures were approved by the Institutional Animal Care and
336 Use Committee at Cincinnati Children's Hospital Medical Center and complied with the National
337 Institutes of Health guidelines. Male C57BL/6J wild type mice aged 6 weeks were purchased
338 from The Jackson Laboratory (Bar Harbor, ME) and entrained to a 12h:12h light dark cycle for 2
339 weeks prior to exposure.

340 *Experimental Design*. All studies were conducted in 8-10 week old male mice. Mice were
341 housed in light boxes and entrained to a 12:12 light:dark cycle for 2 weeks prior to initiation of
342 IH. Mice were randomly assigned to IH or room air exposures. For the experimental group, mice
343 were maintained in a commercially-designed gas control delivery system (Model A84XOV,
344 BioSpherix, Parish, NY) during the inactive (light) phase from (ZT 0-12). Mice were provided
345 with food and water *ad libitum*. For each episode of IH, the fractional inhaled oxygen (O_2) was
346 reduced from 20.9% to 6% over a 50 s exposure period, followed by an immediate 50 s
347 recovery period to 20.9%. The fractional oxygen was maintained at 20.9% for approximately 15
348 s before the cycle was repeated, allowing for ~30 hypoxic events per hour. Ambient temperature
349 in the hypoxia chamber was maintained between 22-24°C to match room air. Mice in the
350 experimental group were maintained at room air during the active phase, ZT 13-24. Mice in the
351 control group were maintained at room air throughout the circadian cycle, ZT 0-24. Experimental
352 and control mice were exposed to IH vs room air for 9 days, followed by sacrifice at ZT 3 on day
353 10 of exposure. This was immediately followed by organ harvest and preparation for bulk RNA-
354 seq, scRNA-seq, or histopathology.
355 *RNA Isolation*. In total, 6 experimental and 6 control mice were used for bulk RNA-seq. For bulk
356 RNA-seq, the lung was quickly harvested and snap-frozen in liquid nitrogen. Organs were later
357 homogenized in TRIzol reagent (Invitrogen) and processed using a bead mill homogenizer
358 (Qiagen Tissuelyser). RNA was then isolated from lung homogenates by phase separation
359 using chloroform and phase separation columns. The aqueous phase was then applied to an
360 RNeasy column following the manufacturer's protocol (Qiagen) to extract and purify the RNA.
361 *Bulk RNA Sequencing and Analysis*. RNA from the lungs of control and experimental mice were
362 sent for bulk sequencing separately. Approximately 0.4 ug of total RNA was used for library
363 preparation. mRNA enrichment and library preparation was performed using the Polyadenylated
364 (PolyA+) mRNA Magnetic Isolation Module (New England Biolabs) and NEBNext Ultra II RNA
365 Library Prep Kit for Illumina (New England Biolabs), following the manufacturer's protocol. All 12

366 samples were then pooled together and sequenced in one lane using Illumina Novaseq 6000
367 platform with paired-end 150bp (table S1). The raw fastq files from RNA-seq were mapped to
368 GRCm38 mouse genome reference using STAR (version 2.5) with default parameters. More
369 than 90% (table S1) of sequenced paired-end reads (above 50M reads for each library) were
370 mapped to the mouse genome by STAR(Dobin et al., 2013). HTSeq(Anders et al., 2015)
371 (version 0.6.0) was used to quantify gene expression, with Ensembl GRCm38.96 as a
372 reference. DESeq2 (version 1.24.0) was used to perform the differential expression analysis on
373 the HTSeq quantified count per gene. The top 200 up and down regulated genes (table S2),
374 ranked by P-value from low to high with fold-change above 1.5 (or log2(fold-change) > 0.58),
375 were used for biological process enrichment analysis in the DAVID database. Biological process
376 terms with at least 5 differentially expressed genes and BHQ < 0.15 were selected. For
377 aggregating redundant biological processes, GOSemSim(Yu et al., 2010) (version 2.10.0) was
378 used to calculate the semantic similarity ('Jiang' method from GOSemSim) between significant
379 biological processes. Redundant biological processes were manually merged into biological
380 process categories (table S3).
381 *Dissociation Protocol for Single Cell Sequencing*. For scRNA-seq, a total of 3 biological
382 replicates (3 IH and 3 controls in the first experiment and 2 of each in the other replicates). On
383 the last day of exposure, the mice were sacrificed, lung harvested, and tissue immediately
384 placed in ice-cold PBS. Dissociation of the pooled whole mouse lung for each group (IH vs RA)
385 was performed as previously described(Guo et al., 2019). Briefly, minced lung was placed in
386 collagenase/elastase/dispase digestion buffer (Sigma-Aldrick, St. Louis, MO; Worthington
387 Biochemical, Lakewood, NJ). After mixing on ice for approximately 3 minutes, the lung was
388 minced again. After resting the suspension, the supernatant was passed through a 30 μM filter.
389 A *Bacillus licheniformis* mix (Sigma-Aldrich) was added to the cell suspension, mixed on ice for
390 approximately 10 min, and passed through a 30 μM filter. The suspension was spun at 500 g for
391 5 min at 4°C. The pellet was rinsed with a red blood cell lysis buffer. This was again passed

392 through a 30 μM filter and then spun at 500 g for 5 min at 4°C. The cell suspension was
393 resuspended in PBS/BSA and manually counted with a hemocytometer. The volume was
394 adjusted to obtain a final concentration of approximately 1000 cells/μL to be loaded to the 10X
395 Chromium platform.
396 *scRNA-seq Library Construction and Sequencing*. The single cell suspension was applied to the
397 10X Genomics Chromium platform (San Francisco, CA) to capture and barcode cells, as
398 described in the manufacturer's protocol. Libraries were constructed using the Single Cell 3'
399 Reagent Kit (v2 Chemistry). The completed libraries were then sequenced using HiSeq 2500
400 (Illumina, San Diego, CA) running in Rapid Mode. Each sample was loaded onto two lanes of a
401 Rapid v2 flow cell.
402 *scRNA-seq Data Processing*. Raw data from 10X Genomics were demultiplexed and converted
403 to a fastq file using cellRanger (v2.1.1) mkfastq. Reads from the same library sequenced in
404 different flow cells (technical replicates) were combined and aligned to the mm10 genome
405 reference using cellRanger count. Summary sentences for statistical mapping are presented in
406 table S4. The gene expression profiles for cells from the three biological replicates of the IH
407 group were combined with cellRanger aggr and were run an unsupervised analysis using the
408 software Iterative Clustering and Guide-gene Selection (ICGS) versions 2 (AltAnalyze version
409 2.1.2) to generate reference clusters using the program defaults with euclidean
410 clustering(DePasquale et al., 2019). ICGS2 grouped 12,324 cells into 25 reference clusters
411 based on the expression profiles of 1,480 selected marker genes (table S5). All cells from
412 control and IH groups were then aligned to these 25 reference clusters using
413 cellHarmony(DePasquale et al., 2019). Uniform Manifold Approximation and Projection (UMAP)
414 calculation was run using integrated function in AltAnalyze -v2.1.2 with default parameters. For
415 annotating the 25 reference clusters into known lung cell-types, we prepared a comprehensive
416 marker gene list for known lung cell types. The sources of this marker gene list included
417 information from the Mouse Cell Atlas, ToppGene, and Lung Gene Expression Analysis

418 (LGEA)(Chen et al., 2009; Consortium et al., 2018; Du et al., 2017). Additionally, we manually
419 collected cell marker genes from published scRNA-seq studies performed in mouse or human
420 lung(Guo et al., 2019; Zilionis et al., 2019). One-tailed Fisher exact test was used to perform
421 enrichment analysis between marker genes for each cluster and the curated reference markers
422 of known lung cell types. Each cluster was manually assigned to a specific cell type based on
423 the known cell type with the lowest BH(Benjamini & Hochberg, 1995) adjusted P-value (GO-
424 Elite software)(Zambon et al., 2012). Those clusters corresponding to the same annotated cell
425 type were manually joined as one cell type for downstream analyses (e.g. endothelial
426 corresponding to four clusters). This process reduced the 25 reference clusters into 19 cell
427 types (table S6). For testing the cell type composition difference of mouse lung between
428 experimental and control groups, a centered log ratio transformation was performed on the
429 percentage of each cell type before applying the t-test (two-tailed). The statistical P-value from
430 the t-test was adjusted with the BH method.

431 *Pseudo-bulk RNA-seq Differential Expression Analysis*. To identify differentially expressed
432 genes in each lung cell type between the control and IH groups with multiple biologic replicates,
433 all cells assigned to the same cell type were aggregated into a “pseudo-bulk” data library by
434 library. For each library, the sum of the reads per gene from cells assigned to the same cell type
435 were used to represent the cell-type-specific gene expression profiles. Percentage of cells
436 expressed per gene were calculated as a fraction of cells with >=1 read(s) for the gene in each
437 cell-type. Count per one million UMI (CPM) for each cell type was calculated as the (sum of
438 reads per gene / sum of reads) * 1000000 for each library. Differential expression analysis was
439 performed with DESeq2 for each cell-type, using the sum of reads per gene as input, with three
440 replicates in each of the control and IH groups. Ranked by P-value from low to high, the top 200
441 up and down regulated genes (table S7) with fold-change above 1.2 (or log2(fold-change) >
442 0.26) were used for biological process enrichment analysis in the DAVID database. Selecting

443 and aggregating biological processes (table S8) were performed as described above in the
444 Methods section labeled, "*Bulk RNA Sequencing and Analysis*." We further extracted those
445 genes enriched in circadian rhythm and immune response, and selected well-established genes
446 in each biological process to demonstrate their expression variation under IH exposure in each
447 cell type based on literature searches.

448 *Endothelial Subpopulations Analysis*. To improve the accuracy for classifying endothelial cells,
449 we reran the AltAnalyze-ICGS2 clustering algorithm using only the 5,579 cells annotated to
450 pulmonary vascular endothelial cells from IH exposure groups, followed by a realignment of all
451 vascular endothelial cells from both control and IH groups to these clusters using cellHarmony.
452 AltAnalyze-ICGS2 produced 6 clusters with 314 marker genes (table S9). We matched the
453 ICGS2 selected marker genes with vascular endothelial subpopulation marker genes presented
454 in a study from Travaglini et al(Travaglini et al., 2019). This annotated the clusters into 4
455 subpopulations of endothelial artery, vein, capillary aerocytes, and general capillary cells (table
456 S10). We further aggregated all cells of the same vascular endothelial subpopulations into
457 "pseudo-bulk" data library by library. DESeq2 was used to detect differentially expressed genes
458 for each subpopulation between the control and IH exposure groups. To select differentially
459 expression genes in each endothelial subpopulation, the cut-off was set as BHQ < 0.2 and fold-
460 change > 1.2 (or log2(fold-change) > 0.26). Those differential expression genes (table S11) in
461 endothelial capillary cells were used for BP enrichment analysis in the DAVID database.
462 Selecting and aggregating biological processes (table S12) were performed as described above
463 in the Methods section labeled, "*Bulk RNA Sequencing and Analysis*."

464 *Association Analysis on IH Responsive Genes with Pulmonary Disease Genes and Drug*
465 *Targets at the Cell-type Level*. Gene-disease association information was downloaded from the
466 DisGeNET(Piñero et al., 2017) database (curated gene-disease associations). The downloaded
467 file was filtered with keywords to specifically select genes linked to pulmonary diseases, which

468 includes“allergic asthma”, “asthma”, “chronic obstructive airway disease”, “pulmonary
469 hypertension”, “chronic thromboembolic pulmonary hypertension”, “idiopathic pulmonary arterial
470 hypertension”, “familial primary pulmonary hypertension”, “idiopathic pulmonary hypertension”,
471 “interstitial lung fibrosis”, “pulmonary fibrosis”, and “idiopathic pulmonary fibrosis”. One-tailed
472 Fisher exact test was used to determine if the top 200 up or down regulated genes in each cell-
473 type exposed to IH significantly overlapped with these pulmonary disease associated genes
474 (table S13). The significant cutoff was set with a BH adjusted P-value from a Fisher exact test <
475 0.05 and at least 5 overlapped genes with any pulmonary disease gene set. For the association
476 analysis between IH responsive genes and pulmonary drug targets, the xml file was
477 downloaded from the DrugBank(Wishart et al., 2008) (version 5.1.4). The drugbankR package
478 (https://github.com/yduan004/drugbankR) was used to parse the xml file to get each drug and
479 its target genes. The parsed drug table was linked with the top 200 up or down regulated genes
480 in each cell-type exposed to IH by drug target genes. The drug table was further filtered with
481 respiratory tissue and disease-associated key words (e.g. asthma, lung, bronchus, airway et al.)
482 to keep candidate drugs used to treat pulmonary diseases. The filtered table was manually
483 curated to select drugs mainly indicated to treat pulmonary diseases. In the association
484 analysis, the ‘homologene’ package (https://github.com/oganm/homologene) was used to find
485 the human-unique homolog of mouse genes. CellPhoneDB is used to predict ligand-receptor
486 interactions between cell-types. The pulmonary diseases relevant drug targeted genes list (Fig
487 6C) is used to select ligand-receptor interaction pairs. Genes with unknown drug effects were
488 filtered out from the analysis. Human homolog gene is used for this analysis. Gain of
489 interactions and loss of interactions is calculated by summing up the number of ligand-receptor
490 interactions that were only significantly present in either hypoxia or control (P-value < 0.05 and
491 mean > 0.1), respectively, for each cell pairs comparison. Two-tailed Fisher exact test was used
492 to calculate significance changes of each cell type. Hive plot is made using the HiveR package
493 (https://github.com/bryanhanson/HiveR).

494 *Lung Fixation, Histological Staining, Immunofluorescence, and Confocal Microscopy.* For
495 histological staining, mice were sacrificed, and lung inflation fixation was immediately
496 performed. After exposure of the trachea and lungs, the trachea was cannulated with a scalp
497 vein cannula (EXELINT, Redondo Beach, CA), and 10% neutral buffered formalin was gravity-
498 perfused into the lung at a height of 25 cm. After infusion, the lung was harvested and placed in
499 formalin for 24 hours. Whole lung was then dehydrated in 70% ethanol and embedded in
500 paraffin. For morphologic evaluation, 5 μm thick sections were cut from the paraffin blocks and
501 stained with hematoxylin and eosin.

502 Immunofluorescence staining on 10% formalin fixed mouse lung was performed on 5 μm
503 thick paraffin embedded tissue sections. Tissue slides were melted at 60°C for two hours,
504 following rehydration through xylene and alcohol, and finally in PBS. Antigen retrieval was
505 performed in 0.1 M citrate buffer (pH 6.0) by microwaving. Slides were blocked for 2 hours at
506 room temperature using 4% normal donkey serum in PBS containing 0.2% Triton X-100, and
507 then incubated with primary antibodies diluted in blocking buffer for approximately 16 hours at
508 4°C. Primary antibodies included ACTA2 (1:2000, Sigma-Aldrich), EMCN (1:200, R&D
509 Systems), FOXFI (1:100, R&D Systems), HOPX (1:100, Santa Cruz Biotechnology), MKI67
510 (1:100, BDBiosciences), POSTN (1:100, ABCAM), Pro-SFTPC (1:1000, Seven Hills
511 Bioreagents), SOX9 (1:100, Millipore), and LYVE1 (1:100, ABCAM). Secondary antibodies
512 conjugated to Alexa Fluor 488, Alexa Fluor 568, or Alexa Fluor 633, were used at a dilution of
513 1:200 in blocking buffer for 1 hour at room temperature. Nuclei were counterstained with DAPI
514 (1μg/ml) (Thermo-Fisher). Sections were mounted using ProLong Gold (Thermo-Fisher)
515 mounting medium and coverslipped. Tissue sections were then imaged on an inverted Nikon
516 A1R confocal microscope using a NA 1.27 objective using a 1.2 AU pinhole. Maximum intensity
517 projections of multi-labeled Z stack images were generated using Nikon NIS-Elements software.

518 **Acknowledgements:** We thank K.A. Wikenheiser-Brokamp for her thoughtful discussion and
519 guidance. We thank Bruce J. Aranow, Yan Xu, Minzhe Guo, Kashish Chetal, and Emily R.
520 Miraldi for their thoughtful discussion about scRNA-seq analysis. We would like to thank S.
521 Steven Potter for allowing us to use resources available in his lab. We would also like to thank
522 Kalpana Srivastava for work on sectioning tissue specimens and completing
523 immunofluorescence assays. **Grant Funding:** This work was supported by Cincinnati Children's
524 Hospital Medical Center, the National Heart, Lung, and Blood Institute (NHLBI; 1 K08
525 HL148551-01), The Triological Society, and the American Society of Pediatric Otolaryngology
526 (ASPO). **Author contributions:** G.W., Y.Y.L., E.M.G., M.D.R., L.J.F., J.B.H., and D.F.S.
527 designed research; G.W., Y.Y.L., E.M.G., A.P., J.K., L.J.F., and D.F.S performed research;
528 G.W., Y.Y.L., N.S., J.A.W., and J.B.H. contributed analytic tools; G.W., Y.Y.L., E.M.G., M.D.R.,
529 N.S., J.A.W., L.J.F., and D.F.S. analyzed data; G.W., Y.Y.L., M.D.R., L.J.F., J.B.H., and D.F.S.
530 wrote this paper. **Data and Materials Availability:** All data associated with this study are
531 present in the paper or the Supplementary Materials and have been incorporated into GEO
532 database (GSE145436).

533 **Competing Interests:** The authors declare that they have no competing interests.

534 **References**

535 Adamovich, Y., Ladeuix, B., Golik, M., Koeners, M. P., & Asher, G. (2017). Rhythmic Oxygen
536 Levels Reset Circadian Clocks through HIF1α. *Cell Metabolism*, *25*(1), 93–101.
537 Aihara, K., Oga, T., Harada, Y., Chihara, Y., Handa, T., Tanizawa, K., Watanabe, K., Tsuboi, T.,
538 Hitomi, T., Mishima, M., & Chin, K. (2011). Comparison of biomarkers of subclinical lung
539 injury in obstructive sleep apnea. *Respiratory Medicine*, *105*(6), 939–945.
540 Amin, R. S., Carroll, J. L., Jeffries, J. L., Grone, C., Bean, J. A., Chini, B., Bokulic, R., & Daniels,
541 S. R. (2004). Twenty-four–hour Ambulatory Blood Pressure in Children with Sleep-
542 disordered Breathing. *American Journal of Respiratory and Critical Care Medicine*, *169*(8),

950–956.

Amin, R. S., Kimball, T. R., Bean, J. A., Jeffries, J. L., Willging, J. P., Cotton, R. T., Witt, S. A., Glascock, B. J., & Daniels, S. R. (2002). Left ventricular hypertrophy and abnormal ventricular geometry in children and adolescents with obstructive sleep apnea. *American Journal of Respiratory and Critical Care Medicine*, *165*(10), 1395–1399.

Amin, R. S., Kimball, T. R., Kalra, M., Jeffries, J. L., Carroll, J. L., Bean, J. A., Witt, S. A., Glascock, B. J., & Daniels, S. R. (2005). Left ventricular function in children with sleep-disordered breathing. *The American Journal of Cardiology*, *95*(6), 801–804.

Anders, S., Pyl, P. T., & Huber, W. (2015). HTSeq--a Python framework to work with high-throughput sequencing data. In *Bioinformatics* (Vol. 31, Issue 2, pp. 166–169). https://doi.org/10.1093/bioinformatics/btu638

Bady, E., Achkar, A., Pascal, S., Orvoen-Frija, E., & Laaban, J. P. (2000). Pulmonary arterial hypertension in patients with sleep apnoea syndrome. *Thorax*, *55*(11), 934–939.

Benjafield, A. V., Ayas, N. T., Eastwood, P. R., Heinzer, R., Ip, M. S. M., Morrell, M. J., Nunez, C. M., Patel, S. R., Penzel, T., Pépin, J.-L., Peppard, P. E., Sinha, S., Tufik, S., Valentine, K., & Malhotra, A. (2019). Estimation of the global prevalence and burden of obstructive sleep apnoea: a literature-based analysis. In *The Lancet Respiratory Medicine* (Vol. 7, Issue 8, pp. 687–698). https://doi.org/10.1016/s2213-2600(19)30198-5

Benjamini, Y., & Hochberg, Y. (1995). Controlling the False Discovery Rate: A Practical and Powerful Approach to Multiple Testing. In *Journal of the Royal Statistical Society: Series B (Methodological)* (Vol. 57, Issue 1, pp. 289–300). https://doi.org/10.1111/j.2517-6161.1995.tb02031.x

Bhattacharjee, R., Kim, J., Alotaibi, W. H., Kheirandish-Gozal, L., Capdevila, O. S., & Gozal, D. (2012). Endothelial dysfunction in children without hypertension: potential contributions of obesity and obstructive sleep apnea. *Chest*, *141*(3), 682–691.

Butler, M. P., Smales, C., Wu, H., Hussain, M. V., Mohamed, Y. A., Morimoto, M., & Shea, S. A.

(2015). The Circadian System Contributes to Apnea Lengthening across the Night in Obstructive Sleep Apnea. *Sleep*, *38*(11), 1793–1801.

Chaouat, A., Weitzenblum, E., Krieger, J., Oswald, M., & Kessler, R. (1996). Pulmonary hemodynamics in the obstructive sleep apnea syndrome. Results in 220 consecutive patients. *Chest*, *109*(2), 380–386.

Chen, J., Bardes, E. E., Aronow, B. J., & Jegga, A. G. (2009). ToppGene Suite for gene list enrichment analysis and candidate gene prioritization. *Nucleic Acids Research*, *37*(Web Server issue), W305–W311.

Consortium, T. T. M., The Tabula Muris Consortium, Coordination, O., Coordination, L., Organ collection and processing, Library preparation and sequencing, Analysis, C. D., Annotation, C. T., Writing group, Supplemental text writing group, & Principal investigators. (2018). Single-cell transcriptomics of 20 mouse organs creates a Tabula Muris. In *Nature* (Vol. 562, Issue 7727, pp. 367–372). https://doi.org/10.1038/s41586-018-0590-4

Cubillos-Zapata, C., Avendaño-Ortiz, J., Hernandez-Jimenez, E., Toledano, V., Casas-Martin, J., Varela-Serrano, A., Torres, M., Almendros, I., Casitas, R., Fernández-Navarro, I., Garcia-Sanchez, A., Aguirre, L. A., Farre, R., López-Collazo, E., & García-Rio, F. (2017). Hypoxia-induced PD-L1/PD-1 crosstalk impairs T-cell function in sleep apnoea. *The European Respiratory Journal: Official Journal of the European Society for Clinical Respiratory Physiology*, *50*(4). https://doi.org/10.1183/13993003.00833-2017

DePasquale, E. A. K., Schnell, D., Dexheimer, P., Ferchen, K., Hay, S., Chetal, K., Valiente-Alandí, Í., Blaxall, B. C., Grimes, H. L., & Salomonis, N. (2019). cellHarmony: cell-level matching and holistic comparison of single-cell transcriptomes. *Nucleic Acids Research*, *47*(21), e138.

Dobin, A., Davis, C. A., Schlesinger, F., Drenkow, J., Zaleski, C., Jha, S., Batut, P., Chaisson, M., & Gingeras, T. R. (2013). STAR: ultrafast universal RNA-seq aligner. *Bioinformatics* , *29*(1), 15–21.

595 Du, Y., Kitzmiller, J. A., Sridharan, A., Perl, A. K., Bridges, J. P., Misra, R. S., Pryhuber, G. S.,
596 Mariani, T. J., Bhattacharya, S., Guo, M., Potter, S. S., Dexheimer, P., Aronow, B., Jobe, A.
597 H., Whitsett, J. A., & Xu, Y. (2017). Lung Gene Expression Analysis (LGEA): an integrative
598 web portal for comprehensive gene expression data analysis in lung development. *Thorax*,
599 *72*(5), 481–484.
600 Edgar, R. S., Green, E. W., Zhao, Y., van Ooijen, G., Olmedo, M., Qin, X., Xu, Y., Pan, M.,
601 Valekunja, U. K., Feeney, K. A., Maywood, E. S., Hastings, M. H., Baliga, N. S., Merrow,
602 M., Millar, A. J., Johnson, C. H., Kyriacou, C. P., O'Neill, J. S., & Reddy, A. B. (2012).
603 Peroxiredoxins are conserved markers of circadian rhythms. In *Nature* (Vol. 485, Issue
604 7399, pp. 459–464). https://doi.org/10.1038/nature11088
605 Eltzschig, H. K., & Carmeliet, P. (2011). Hypoxia and inflammation. *The New England Journal of*
606 *Medicine*, *364*(7), 656–665.
607 Enright, P. L., Goodwin, J. L., Sherrill, D. L., Quan, J. R., & Quan, S. F. (2003). Tucson
608 children's assessment of sleep apnea study. *Blood Pressure Elevation Associated with*
609 *Sleep-Related Breathing Disorder in a Community Sample of White and Hispanic Children:*
610 *The Tucson Children's Assessment of Sleep Apnea Study. Arch Pediatr Adolesc Med*,
611 *157*(9), 901–904.
612 Entzian, P., Linnemann, K., Schlaak, M., & Zabel, P. (1996). Obstructive sleep apnea syndrome
613 and circadian rhythms of hormones and cytokines. *American Journal of Respiratory and*
614 *Critical Care Medicine*, *153*(3), 1080–1086.
615 Farber, H. W., & Gin-Sing, W. (2016). Practical considerations for therapies targeting the
616 prostacyclin pathway. *European Respiratory Review: An Official Journal of the European*
617 *Respiratory Society*, *25*(142), 418–430.
618 Gibbs, J. E., Beesley, S., Plumb, J., Singh, D., Farrow, S., Ray, D. W., & Loudon, A. S. I.
619 (2009). Circadian timing in the lung; a specific role for bronchiolar epithelial cells.
620 *Endocrinology*, *150*(1), 268–276.

621 Gille, T., Didier, M., Rotenberg, C., Delbrel, E., Marchant, D., Sutton, A., Dard, N., Haine, L.,
622 Voituron, N., Bernaudin, J.-F., Valeyre, D., Nunes, H., Besnard, V., Boncoeur, E., & Planès,
623 C. (2018). Intermittent Hypoxia Increases the Severity of Bleomycin-Induced Lung Injury in
624 Mice. *Oxidative Medicine and Cellular Longevity*, *2018*, 1240192.
625 Gottlieb, D. J., Yenokyan, G., Newman, A. B., O'Connor, G. T., Punjabi, N. M., Quan, S. F.,
626 Redline, S., Resnick, H. E., Tong, E. K., Diener-West, M., & Shahar, E. (2010). Prospective
627 Study of Obstructive Sleep Apnea and Incident Coronary Heart Disease and Heart Failure.
628 *Circulation*, *122*(4), 352–360.
629 Gozal, D., Serpero, L. D., Sans Capdevila, O., & Kheirandish-Gozal, L. (2008). Systemic
630 inflammation in non-obese children with obstructive sleep apnea. *Sleep Medicine*, *9*(3),
631 254–259.
632 Guo, M., Du, Y., Gokey, J. J., Ray, S., Bell, S. M., Adam, M., Sudha, P., Perl, A. K., Deshmukh,
633 H., Potter, S. S., Whitsett, J. A., & Xu, Y. (2019). Single cell RNA analysis identifies cellular
634 heterogeneity and adaptive responses of the lung at birth. *Nature Communications*, *10*(1),
635 37.
636 Gu, Y. Z., Hogenesch, J. B., & Bradfield, C. A. (2000). The PAS superfamily: sensors of
637 environmental and developmental signals. *Annual Review of Pharmacology and*
638 *Toxicology*, *40*, 519–561.
639 Hersh, C. P., DeMeo, D. L., Raby, B. A., Litonjua, A. A., Sylvia, J. S., Sparrow, D., Reilly, J. J., &
640 Silverman, E. K. (2006). Genetic linkage and association analysis of COPD-related traits on
641 chromosome 8p. *COPD*, *3*(4), 189–194.
642 Hogenesch, J. B., Gu, Y.-Z., Jain, S., & Bradfield, C. A. (1998). The basic-helix–loop–helix-PAS
643 orphan MOP3 forms transcriptionally active complexes with circadian and hypoxia factors.
644 *Proceedings of the National Academy of Sciences*, *95*(10), 5474–5479.
645 Huang, D. W., Sherman, B. T., & Lempicki, R. A. (2009). Systematic and integrative analysis of
646 large gene lists using DAVID bioinformatics resources. *Nature Protocols*, *4*(1), 44–57.

Idell, S., Maunder, R., Fein, A. M., Switalska, H. I., Tuszynski, G. F., McLarty, J., & Niewiarowski, S. (1989). Platelet-specific α-Granule Proteins and Thrombospondin in Bronchoalveolar Lavage in the Adult Respiratory Distress Syndrome. In *Chest* (Vol. 96, Issue 5, pp. 1125–1132). https://doi.org/10.1378/chest.96.5.1125

Kheirandish-Gozal, L., Khalyfa, A., Gozal, D., Bhattacharjee, R., & Wang, Y. (2013). Endothelial dysfunction in children with obstructive sleep apnea is associated with epigenetic changes in the eNOS gene. *Chest*, *143*(4), 971–977.

Kim, J. S., Podolanczuk, A. J., Borker, P., Kawut, S. M., Raghu, G., Kaufman, J. D., Stukovsky, K. D. H., Hoffman, E. A., Barr, R. G., Gottlieb, D. J., Redline, S. S., & Lederer, D. J. (2017). Obstructive Sleep Apnea and Subclinical Interstitial Lung Disease in the Multi-Ethnic Study of Atherosclerosis (MESA). *Annals of the American Thoracic Society*, *14*(12), 1786–1795.

King, D. P., Zhao, Y., Sangoram, A. M., Wilsbacher, L. D., Tanaka, M., Antoch, M. P., Steeves, T. D. L., Vitaterna, M. H., Kornhauser, J. M., Lowrey, P. L., & Others. (1997). Positional cloning of the mouse circadian clockgene. *Cell*, *89*(4), 641–653.

Kobayashi, M., Morinibu, A., Koyasu, S., Goto, Y., Hiraoka, M., & Harada, H. (2017). A circadian clock gene, PER2, activates HIF-1 as an effector molecule for recruitment of HIF-1α to promoter regions of its downstream genes. *The FEBS Journal*, *284*(22), 3804–3816.

Kohyama, J., Ohinata, J. S., & Hasegawa, T. (2003). Blood pressure in sleep disordered breathing. *Archives of Disease in Childhood*, *88*(2), 139–142.

Kuhn, C., & Mason, R. J. (1995). Immunolocalization of SPARC, tenascin, and thrombospondin in pulmonary fibrosis. *The American Journal of Pathology*, *147*(6), 1759–1769.

Lam, D. C. L., & Ip, M. S. M. (2019). Sleep apnoea and immune regulation: The story is only beginning [Review of *Sleep apnoea and immune regulation: The story is only beginning*]. *Respirology* , *24*(7), 624–625.

Lancaster, L. H., Mason, W. R., Parnell, J. A., Rice, T. W., Loyd, J. E., Milstone, A. P., Collard, H. R., & Malow, B. A. (2009). Obstructive sleep apnea is common in idiopathic pulmonary

673 fibrosis. *Chest*, *136*(3), 772–778.

674 Lederer, D. J., Jelic, S., Basner, R. C., Ishizaka, A., & Bhattacharya, J. (2009). Circulating KL-6,
675 a biomarker of lung injury, in obstructive sleep apnoea. *The European Respiratory Journal:*
676 *Official Journal of the European Society for Clinical Respiratory Physiology*, *33*(4), 793–
677 796.

678 Li, Li, L., Zhang, S., Wei, L., Wang, Z., Ma, W., Liu, F., & Qian, Y. (2018). FGF2 and FGFR2 in
679 patients with idiopathic pulmonary fibrosis and lung cancer. In *Oncology Letters*.
680 https://doi.org/10.3892/ol.2018.8903

681 Love, M. I., Huber, W., & Anders, S. (2014). Moderated estimation of fold change and
682 dispersion for RNA-seq data with DESeq2. In *Genome Biology* (Vol. 15, Issue 12).
683 https://doi.org/10.1186/s13059-014-0550-8

684 Manella, G., Aviram, R., Bolshette, N., Muvkadi, S., Golik, M., Smith, D. F., & Asher, G. (2020).
685 Hypoxia induces a time- and tissue-specific response that elicits intertissue circadian clock
686 misalignment. In *Proceedings of the National Academy of Sciences* (Vol. 117, Issue 1, pp.
687 779–786). https://doi.org/10.1073/pnas.1914112117

688 Marcus, C. L., Brooks, L. J., Draper, K. A., Gozal, D., Halbower, A. C., Jones, J., Schechter, M.
689 S., Ward, S. D., Sheldon, S. H., Shiffman, R. N., Lehmann, C., Spruyt, K., & American
690 Academy of Pediatrics. (2012). Diagnosis and management of childhood obstructive sleep
691 apnea syndrome. *Pediatrics*, *130*(3), e714–e755.

692 Marin, J. M., Agusti, A., Villar, I., Forner, M., Nieto, D., Carrizo, S. J., Barbé, F., Vicente, E., Wei,
693 Y., Javier Nieto, F., & Jelic, S. (2012). Association Between Treated and Untreated
694 Obstructive Sleep Apnea and Risk of Hypertension. In *JAMA* (Vol. 307, Issue 20).
695 https://doi.org/10.1001/jama.2012.3418

696 McIntosh, B. E., Hogenesch, J. B., & Bradfield, C. A. (2010). Mammalian Per-Arnt-Sim proteins
697 in environmental adaptation. *Annual Review of Physiology*, *72*, 625–645.

698 McNicholas, W. T. (2009). Chronic obstructive pulmonary disease and obstructive sleep apnea:

699 overlaps in pathophysiology, systemic inflammation, and cardiovascular disease. *American*
700 *Journal of Respiratory and Critical Care Medicine*, *180*(8), 692–700.
701 Nisbet, R. E., Graves, A. S., Kleinhenz, D. J., Rupnow, H. L., Reed, A. L., Fan, T.-H. M.,
702 Mitchell, P. O., Sutliff, R. L., & Hart, C. M. (2009). The role of NADPH oxidase in chronic
703 intermittent hypoxia-induced pulmonary hypertension in mice. *American Journal of*
704 *Respiratory Cell and Molecular Biology*, *40*(5), 601–609.
705 Osorio, R. S., Gumb, T., Pirraglia, E., Varga, A. W., -e. Lu, S., Lim, J., Wohlleber, M. E., Ducca,
706 E. L., Koushyk, V., Glodzik, L., Mosconi, L., Ayappa, I., Rapoport, D. M., de Leon, M. J.,
707 Weiner, M. W., Aisen, P., Petersen, R., Jack, C., Jagust, W., … For the Alzheimer's
708 Disease Neuroimaging Initiative. (2015). Sleep-disordered breathing advances cognitive
709 decline in the elderly. In *Neurology* (Vol. 84, Issue 19, pp. 1964–1971).
710 https://doi.org/10.1212/wnl.0000000000001566
711 Peek, C. B., Levine, D. C., Cedernaes, J., Taguchi, A., Kobayashi, Y., Tsai, S. J., Bonar, N. A.,
712 McNulty, M. R., Ramsey, K. M., & Bass, J. (2017). Circadian Clock Interaction with HIF1α
713 Mediates Oxygenic Metabolism and Anaerobic Glycolysis in Skeletal Muscle. *Cell*
714 *Metabolism*, *25*(1), 86–92.
715 Perl, A.-K. T., & Gale, E. (2009). FGF signaling is required for myofibroblast differentiation
716 during alveolar regeneration. *American Journal of Physiology. Lung Cellular and Molecular*
717 *Physiology*, *297*(2), L299–L308.
718 Peyssonnaux, C., Datta, V., Cramer, T., Doedens, A., Theodorakis, E. A., Gallo, R. L., Hurtado-
719 Ziola, N., Nizet, V., & Johnson, R. S. (2005). HIF-1α expression regulates the bactericidal
720 capacity of phagocytes. In *Journal of Clinical Investigation* (Vol. 115, Issue 7, pp. 1806–
721 1815). https://doi.org/10.1172/jci23865
722 Piñero, J., Bravo, À., Queralt-Rosinach, N., Gutiérrez-Sacristán, A., Deu-Pons, J., Centeno, E.,
723 García-García, J., Sanz, F., & Furlong, L. I. (2017). DisGeNET: a comprehensive platform
724 integrating information on human disease-associated genes and variants. *Nucleic Acids*

725 *Research*, *45*(D1), D833–D839.
726 Plasschaert, L. W., Žilionis, R., Choo-Wing, R., Savova, V., Knehr, J., Roma, G., Klein, A. M., &
727 Jaffe, A. B. (2018). A single-cell atlas of the airway epithelium reveals the CFTR-rich
728 pulmonary ionocyte. *Nature*. https://doi.org/10.1038/s41586-018-0394-6
729 Punjabi, N. M., & Beamer, B. A. (2009). Alterations in Glucose Disposal in Sleep-disordered
730 Breathing. *American Journal of Respiratory and Critical Care Medicine*, *179*(3), 235–240.
731 Reinke, C., Bevans-Fonti, S., Grigoryev, D. N., Drager, L. F., Myers, A. C., Wise, R. A.,
732 Schwartz, A. R., Mitzner, W., & Polotsky, V. Y. (2011). Chronic intermittent hypoxia induces
733 lung growth in adult mice. *American Journal of Physiology. Lung Cellular and Molecular*
734 *Physiology*, *300*(2), L266–L273.
735 Ren, X., Ustiyan, V., Guo, M., Wang, G., Bolte, C., Zhang, Y., Xu, Y., Whitsett, J. A., Kalin, T.
736 V., & Kalinichenko, V. V. (2019). Postnatal Alveologenesis Depends on FOXF1 Signaling in
737 c-KIT Endothelial Progenitor Cells. In *American Journal of Respiratory and Critical Care*
738 *Medicine* (Vol. 200, Issue 9, pp. 1164–1176). https://doi.org/10.1164/rccm.201812-2312oc
739 Sajkov, D., & McEvoy, R. D. (2009). Obstructive sleep apnea and pulmonary hypertension.
740 *Progress in Cardiovascular Diseases*, *51*(5), 363–370.
741 Sajkov, D., Wang, T., Saunders, N. A., Bune, A. J., Neill, A. M., & Douglas Mcevoy, R. (1999).
742 Daytime pulmonary hemodynamics in patients with obstructive sleep apnea without lung
743 disease. *American Journal of Respiratory and Critical Care Medicine*, *159*(5 Pt 1), 1518–
744 1526.
745 Scholz, C. C., & Taylor, C. T. (2013). Targeting the HIF pathway in inflammation and immunity.
746 In *Current Opinion in Pharmacology* (Vol. 13, Issue 4, pp. 646–653).
747 https://doi.org/10.1016/j.coph.2013.04.009
748 Shiraishi, T., Verdone, J. E., Huang, J., Kahlert, U. D., Hernandez, J. R., Torga, G., Zarif, J. C.,
749 Epstein, T., Gatenby, R., McCartney, A., Elisseeff, J. H., Mooney, S. M., An, S. S., &
750 Pienta, K. J. (2015). Glycolysis is the primary bioenergetic pathway for cell motility and

751 cytoskeletal remodeling in human prostate and breast cancer cells. In *Oncotarget* (Vol. 6,
752 Issue 1). https://doi.org/10.18632/oncotarget.2766
753 Silverman, E. K., Palmer, L. J., Mosley, J. D., Barth, M., Senter, J. M., Brown, A., Drazen, J. M.,
754 Kwiatkowski, D. J., Chapman, H. A., Campbell, E. J., Province, M. A., Rao, D. C., Reilly, J.
755 J., Ginns, L. C., Speizer, F. E., & Weiss, S. T. (2002). Genomewide Linkage Analysis of
756 Quantitative Spirometric Phenotypes in Severe Early-Onset Chronic Obstructive Pulmonary
757 Disease. In *The American Journal of Human Genetics* (Vol. 70, Issue 5, pp. 1229–1239).
758 https://doi.org/10.1086/340316
759 Sitbon, O., & Vonk Noordegraaf, A. (2017). Epoprostenol and pulmonary arterial hypertension:
760 20 years of clinical experience. *European Respiratory Review: An Official Journal of the*
761 *European Respiratory Society*, *26*(143). https://doi.org/10.1183/16000617.0055-2016
762 Smith, D. F., Hossain, M. M., Hura, A., Huang, G., McConnell, K., Ishman, S. L., & Amin, R. S.
763 (2017). Inflammatory Milieu and Cardiovascular Homeostasis in Children with Obstructive
764 Sleep Apnea. *Sleep*. https://doi.org/10.1093/sleep/zsx022
765 Sullivan, F. (2016). Hidden Health Crisis Costing America Billions: Underdiagnosing and
766 Undertreating Obstructive Sleep Apnea Draining Healthcare System. *Journal of Clinical*
767 *Sleep Medicine: JCSM: Official Publication of the American Academy of Sleep Medicine*.
768 Tauman, R., Lavie, L., Greenfeld, M., & Sivan, Y. (2014). Oxidative stress in children with
769 obstructive sleep apnea syndrome. *Journal of Clinical Sleep Medicine: JCSM: Official*
770 *Publication of the American Academy of Sleep Medicine*, *10*(6), 677–681.
771 Taylor, B. L., & Zhulin, I. B. (1999). PAS domains: internal sensors of oxygen, redox potential,
772 and light. *Microbiology and Molecular Biology Reviews: MMBR*, *63*(2), 479–506.
773 Taylor, C. T., Doherty, G., Fallon, P. G., & Cummins, E. P. (2016). Hypoxia-dependent
774 regulation of inflammatory pathways in immune cells. *The Journal of Clinical Investigation*,
775 *126*(10), 3716–3724.
776 Travaglini, K. J., Nabhan, A. N., Penland, L., & Sinha, R. (2019). A molecular cell atlas of the

human lung from single cell RNA sequencing. *bioRxiv*. https://www.biorxiv.org/content/10.1101/742320v1.abstract

Tuleta, I., Stöckigt, F., Juergens, U. R., Pizarro, C., Schrickel, J. W., Kristiansen, G., Nickenig, G., & Skowasch, D. (2016). Intermittent Hypoxia Contributes to the Lung Damage by Increased Oxidative Stress, Inflammation, and Disbalance in Protease/Antiprotease System. *Lung*, *194*(6), 1015–1020.

Valham, F., Mooe, T., Rabben, T., Stenlund, H., Wiklund, U., & Franklin, K. A. (2008). Increased Risk of Stroke in Patients With Coronary Artery Disease and Sleep Apnea. In *Circulation* (Vol. 118, Issue 9, pp. 955–960). https://doi.org/10.1161/circulationaha.108.783290

Vento-Tormo, R., Efremova, M., Botting, R. A., Turco, M. Y., Vento-Tormo, M., Meyer, K. B., Park, J.-E., Stephenson, E., Polański, K., Goncalves, A., Gardner, L., Holmqvist, S., Henriksson, J., Zou, A., Sharkey, A. M., Millar, B., Innes, B., Wood, L., Wilbrey-Clark, A., … Teichmann, S. A. (2018). Single-cell reconstruction of the early maternal–fetal interface in humans. *Nature*, *563*(7731), 347–353.

von Allmen, D. C., Francey, L. J., Rogers, G. M., Ruben, M. D., Cohen, A. P., Wu, G., Schmidt, R. E., Ishman, S. L., Amin, R. S., Hogenesch, J. B., & Smith, D. F. (2018). Circadian Dysregulation: The Next Frontier in Obstructive Sleep Apnea Research. *Otolaryngology--Head and Neck Surgery: Official Journal of American Academy of Otolaryngology-Head and Neck Surgery*, 194599818797311.

Walmsley, S. R., Print, C., Farahi, N., Peyssonnaux, C., Johnson, R. S., Cramer, T., Sobolewski, A., Condliffe, A. M., Cowburn, A. S., Johnson, N., & Chilvers, E. R. (2005). Hypoxia-induced neutrophil survival is mediated by HIF-1alpha-dependent NF-kappaB activity. *The Journal of Experimental Medicine*, *201*(1), 105–115.

Wishart, D. S., Knox, C., Guo, A. C., Cheng, D., Shrivastava, S., Tzur, D., Gautam, B., & Hassanali, M. (2008). DrugBank: a knowledgebase for drugs, drug actions and drug targets. *Nucleic Acids Research*, *36*(Database issue), D901–D906.

803 Wohlrab, P., Soto-Gonzales, L., Benesch, T., Winter, M. P., Lang, I. M., Markstaller, K., Tretter,
804 V., & Klein, K. U. (2018). Intermittent Hypoxia Activates Duration-Dependent Protective and
805 Injurious Mechanisms in Mouse Lung Endothelial Cells. *Frontiers in Physiology*, *9*, 1754.
806 Wu, Y., Tang, D., Liu, N., Xiong, W., Huang, H., Li, Y., Ma, Z., Zhao, H., Chen, P., Qi, X., &
807 Zhang, E. E. (2017). Reciprocal Regulation between the Circadian Clock and Hypoxia
808 Signaling at the Genome Level in Mammals. *Cell Metabolism*, *25*(1), 73–85.
809 Xu, Y., Mizuno, T., Sridharan, A., Du, Y., Guo, M., Tang, J., Wikenheiser-Brokamp, K. A., Perl,
810 A.-K. T., Funari, V. A., Gokey, J. J., Stripp, B. R., & Whitsett, J. A. (2016). Single-cell RNA
811 sequencing identifies diverse roles of epithelial cells in idiopathic pulmonary fibrosis. *JCI*
812 *Insight*, *1*(20), e90558.
813 Yehualaeshet, T., O'Connor, R., Begleiter, A., Murphy-Ullrich, J. E., Silverstein, R., & Khalil, N.
814 (2000). A CD36 synthetic peptide inhibits bleomycin-induced pulmonary inflammation and
815 connective tissue synthesis in the rat. *American Journal of Respiratory Cell and Molecular*
816 *Biology*, *23*(2), 204–212.
817 Yu, G., Li, F., Qin, Y., Bo, X., Wu, Y., & Wang, S. (2010). GOSemSim: an R package for
818 measuring semantic similarity among GO terms and gene products. In *Bioinformatics* (Vol.
819 26, Issue 7, pp. 976–978). https://doi.org/10.1093/bioinformatics/btq064
820 Zambon, A. C., Gaj, S., Ho, I., Hanspers, K., Vranizan, K., Evelo, C. T., Conklin, B. R., Pico, A.
821 R., & Salomonis, N. (2012). GO-Elite: a flexible solution for pathway and ontology over-
822 representation. *Bioinformatics* , *28*(16), 2209–2210.
823 Zhang, M. J., Ntranos, V., & Tse, D. (2018). One read per cell per gene is optimal for single-cell
824 RNA-Seq. In *bioRxiv* (p. 389296). https://doi.org/10.1101/389296
825 Zhang, Z., Hunter, L., Wu, G., Maidstone, R., Mizoro, Y., Vonslow, R., Fife, M., Hopwood, T.,
826 Begley, N., Saer, B., Wang, P., Cunningham, P., Baxter, M., Durrington, H., Blaikley, J. F.,
827 Hussell, T., Rattray, M., Hogenesch, J. B., Gibbs, J., … Loudon, A. S. I. (2019). Genome-
828 wide effect of pulmonary airway epithelial cell–specific Bmal1 deletion. *The FASEB Journal*,

829 *33*(5), 6226–6238.

830 Zhou, Y.-D., -D. Zhou, Y., Barnard, M., Tian, H., Li, X., Ring, H. Z., Francke, U., Shelton, J.,
831 Richardson, J., Russell, D. W., & McKnight, S. L. (1997). Molecular characterization of two
832 mammalian bHLH-PAS domain proteins selectively expressed in the central nervous
833 system. In *Proceedings of the National Academy of Sciences* (Vol. 94, Issue 2, pp. 713–
834 718). https://doi.org/10.1073/pnas.94.2.713

835 Zilionis, R., Engblom, C., Pfirschke, C., Savova, V., Zemmour, D., Saatcioglu, H. D., Krishnan,
836 I., Maroni, G., Meyerovitz, C. V., Kerwin, C. M., Choi, S., Richards, W. G., De Rienzo, A.,
837 Tenen, D. G., Bueno, R., Levantini, E., Pittet, M. J., & Klein, A. M. (2019). Single-Cell
838 Transcriptomics of Human and Mouse Lung Cancers Reveals Conserved Myeloid
839 Populations across Individuals and Species. *Immunity*, *50*(5), 1317–1334.e10.

Figures

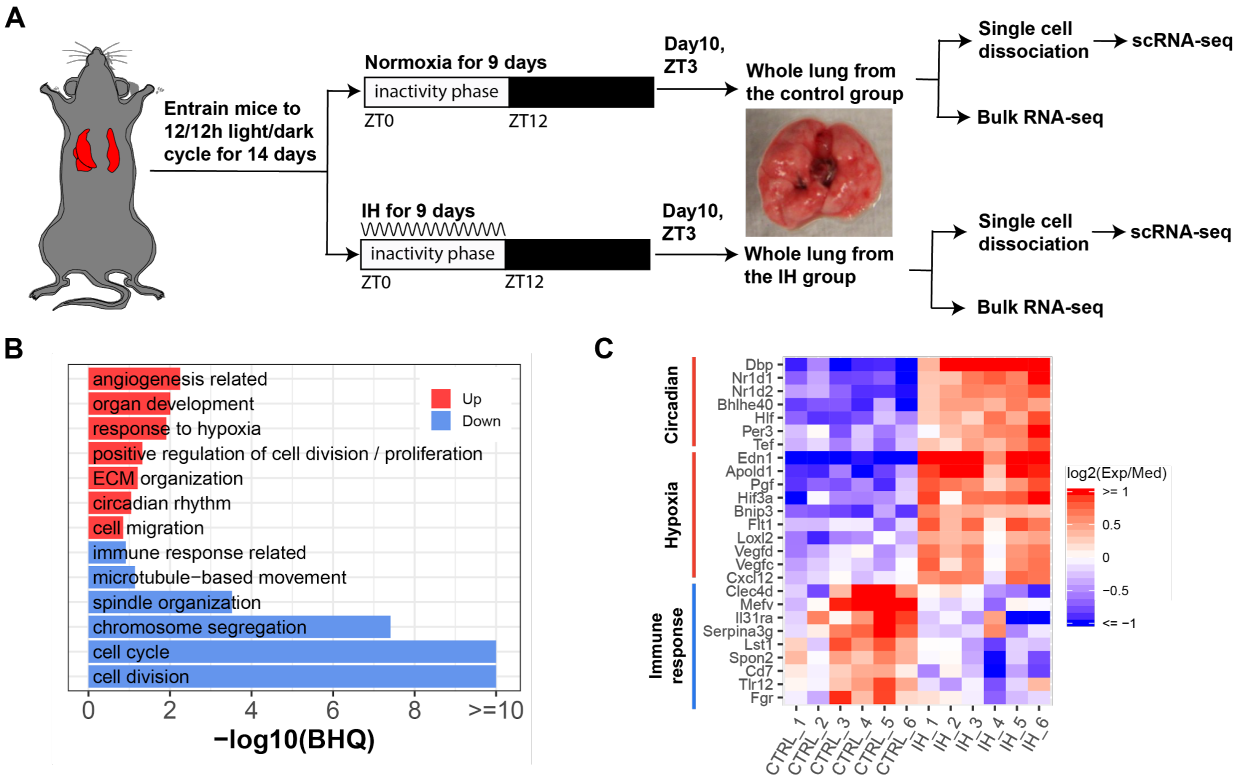

Fig. 1. Short-term exposure to intermittent hypoxia reshapes circadian and immune pathways in the lung. (A) Schematic of IH protocol. Mice are entrained to the same 12 h:12 h light:dark cycle for 14 days prior to IH exposure. Mice are exposed to normoxia (controls) or intermittent episodes of hypoxia (21 to 6% oxygen saturation) followed by recovery to 21% oxygen over the entire 12 h inactivity phase for 9 days. Mice are then sacrificed at ZT 3 (3 h after lights-on) on the 10th day for tissue harvest. Bulk RNA-seq and scRNA-seq were performed for each group. (B) Biological processes enriched in lung from mice exposed to IH vs controls. Enrichment analysis was performed in the DAVID database, using the top 200 up and down regulated genes identified from differential expression analyses. Redundant biological processes are merged into one category. Biological processes enriched in up and down regulated genes are indicated in red and blue bars, respectively. (C) The heatmap shows the fold change of associated genes in circadian rhythm, response to hypoxia, and immune response. The red and blue indicates up and down regulated genes in the experimental group. There are six biological replicates for each group.

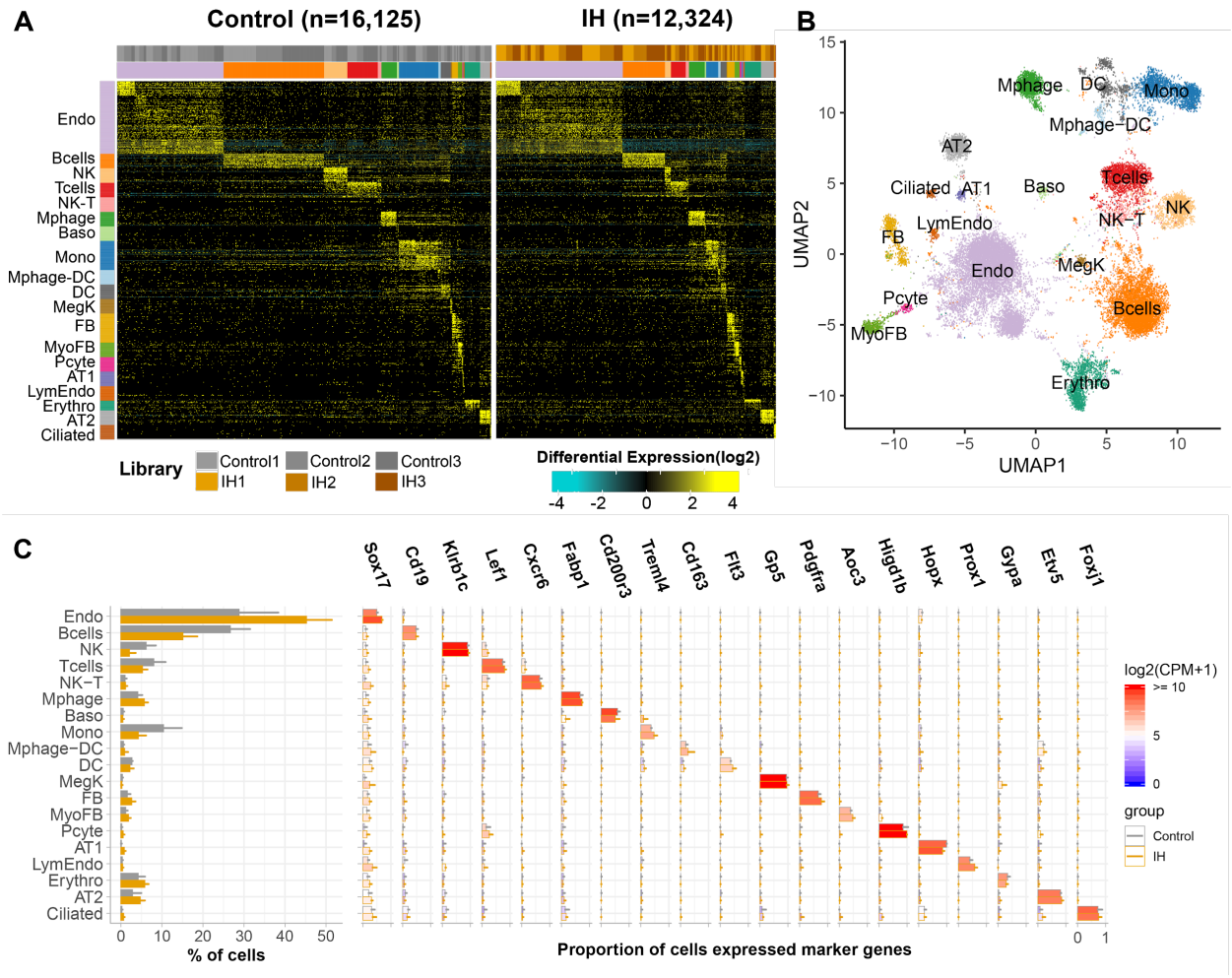

Fig. 2. Single cell sequencing identifies 19 distinct cell types in the lungs of intermittent hypoxia and control mice. (A) Heat map of AltAnalyze selected marker genes for each cell population. Columns and rows represent individual cells and marker genes, respectively. Biological replicates and cell types are indicated by the color bars on the top. cellHarmony was used to align cells from control to IH groups. (B) UMAP projection of whole lung cell populations from IH and control mice in the heatmap. (C) Percentage (left panel) and expression of marker genes (right panel) for each cell type from experimental and control mice. Error bars indicate standard deviation of cell proportion from the three replicates. The list of cell types include: endothelial cells (Endo), B cells (Bcells), natural killer cells (NK), T cells (Tcells), natural killer cells (NK), natural killer T cells (NK-T), macrophages (Mphage), basophils (Baso), monocytes (Mono), macrophages-dendritic CD163+ cells (Mphage-DC), dendritic cells (DC), megakaryocytes (MegK), fibroblasts (FB), myofibroblasts (MyoFB), pericytes (Pcyte), alveolar type I cells (AT1), lymphatic endothelial cells (LympEndo), erythroblasts (Erythro), alveolar type II cells (AT2), and ciliated cells (Ciliated). CPM indicates UMI count per million.

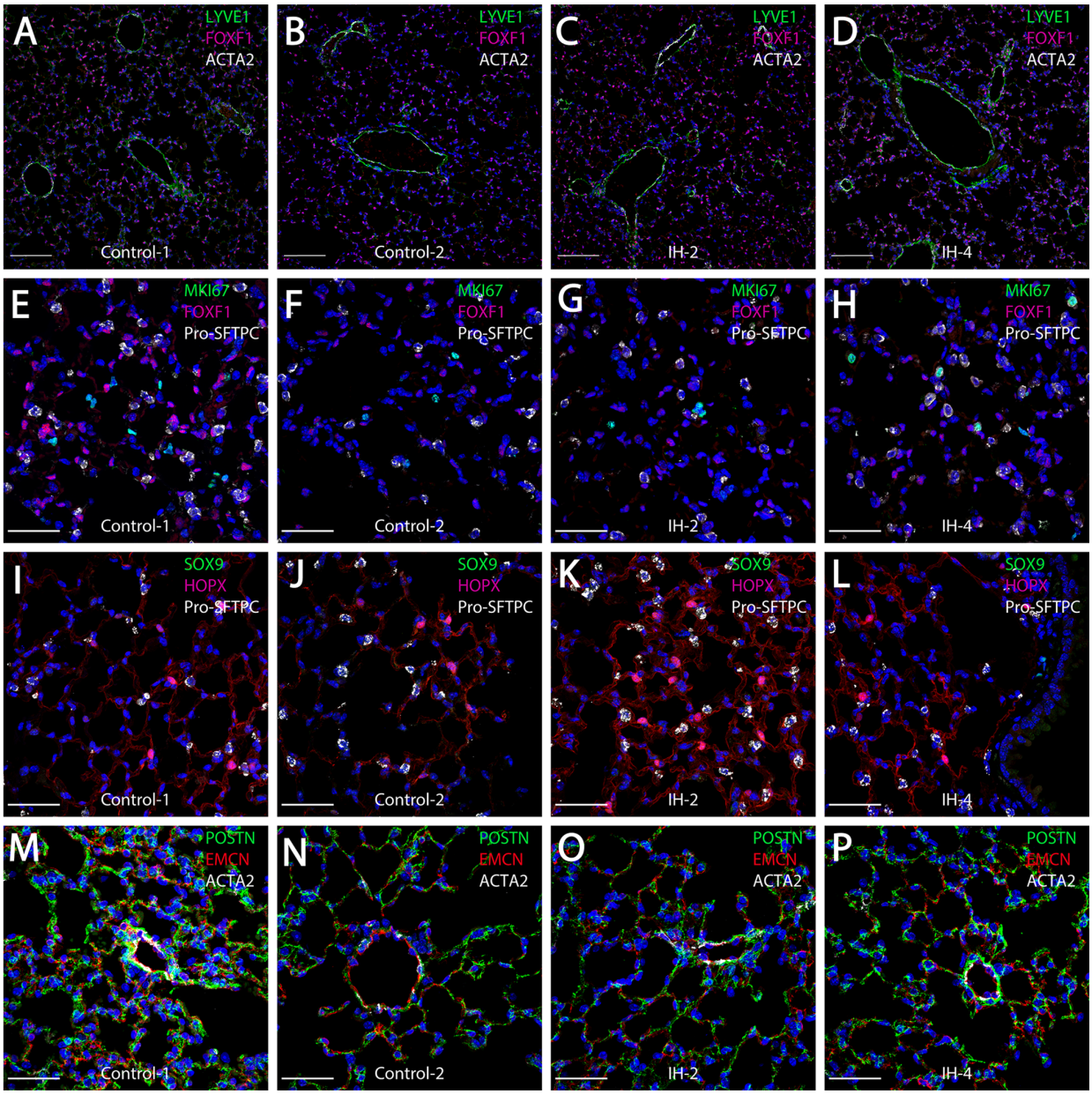

Fig. 3. Short-term exposure to intermittent hypoxia did not lead to histologic changes in the lung. (A-D) Immunostaining for LYVE1, FOXF1, and ACTA2 in mouse lung show no changes in the number or clustering of endothelial cells. (E-H) Immunostaining for MKI67, FOXF1, and Pro-SFTPC did not show changes in the number of proliferating endothelial cells. (I-L) Expression levels of SOX9, HOPX, and Pro-SFTPC did not demonstrate differences in the number of progenitor cells, alveolar type I cells, or alveolar type II cells. (M-P) Immunostaining for POSTN, EMCN, and ACTA2 in mouse lung did not show IH-induced changes in extracellular matrix markers. The scale bars for A-D represent 100 μm. The scale bars for E-P represent 40 μm. KEY: LYVE1 is expressed at high levels in lymphatic and vascular endothelial cells. FOXF1 and ACTA2 are expressed at high levels in vascular endothelial and smooth muscle cells, respectively. MKI67 is a marker for cell proliferation. HOPX and Pro-SFTPC show high expression levels in the alveolar type I cells and alveolar type II cells, respectively. SOX9 is a marker for progenitor cells. POSTN is used to stain extracellular matrix. EMCN is a marker for capillaries and veins/venules.

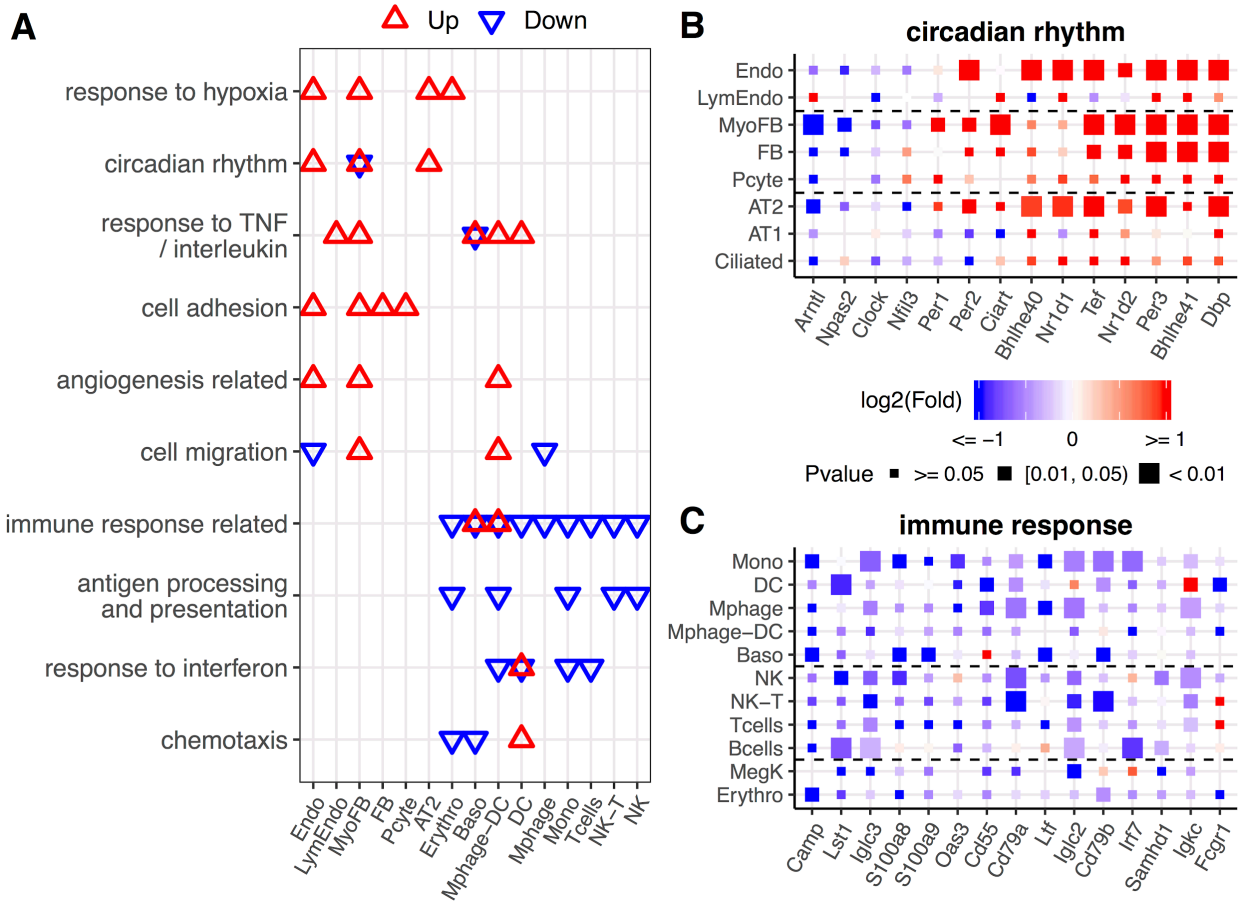

Fig. 4. Diverse expression pathways were up and down regulated in the presence of intermittent hypoxia. (A) Biological processes enriched in different cell types from lungs of mice exposed to IH vs Control. Enrichment analysis was performed in the DAVID database, using the top 200 up and down regulated genes identified from each cell type. Redundant biological processes are merged into one category. Biological processes enriched in up and down regulated genes are indicated in red and blue triangles, respectively. (B) Expression variation of well-established genes involved in circadian rhythm for endothelial, epithelial, and mesenchymal cells. (C) Expression variation of well-established genes involved in immune response for immune associated cells. For B and C, the fold change is indicated by the color, and the P-value for differential expression is indicated by the point size. The list of cell types include: endothelial cells (Endo), B cells (Bcells), natural killer cells (NK), T cells (Tcells), natural killer cells (NK), natural killer T cells (NK-T), macrophages (Mphage), basophils (Baso), monocytes (Mono), macrophages-dendritic CD163+ cells (Mphage-DC), dendritic cells (DC), megakaryocytes (MegK), fibroblasts (FB), myofibroblasts (MyoFB), pericytes (Pcyte), alveolar type I cells (AT1), lymphatic endothelial cells (LympEndo), erythroblasts (Erythro), alveolar type II cells (AT2), and ciliated cells (Ciliated).

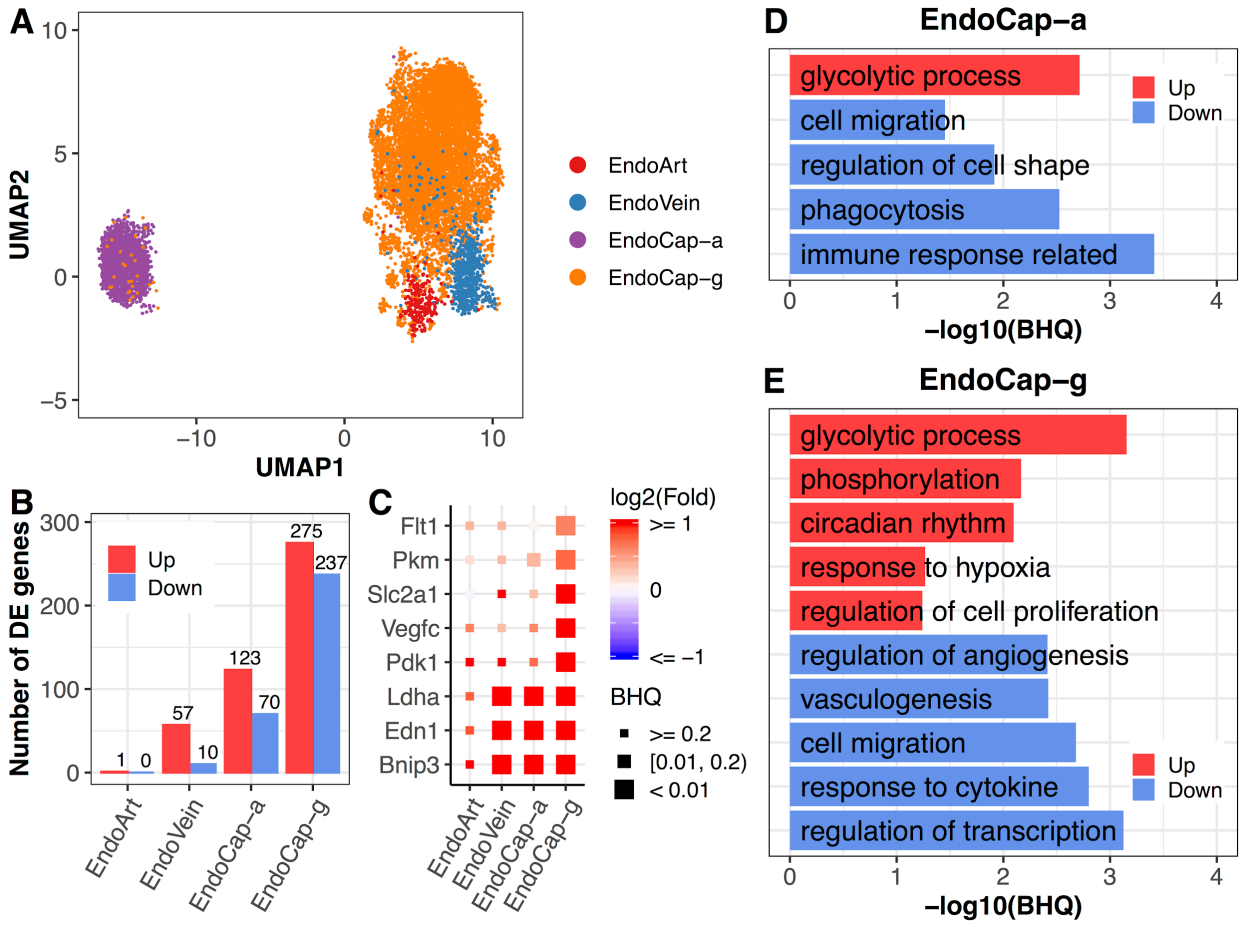

Fig. 5. Pulmonary vascular endothelial subpopulations show distinctive responses to intermittent hypoxia. (A) UMAP projection of cells from four lung endothelial subpopulations. (B) The number of differentially expressed (BHQ < 0.2) genes in each endothelial subpopulation from IH vs control. (C) Expression variation of related genes in response to IH is shown for each endothelial subpopulation. Biological processes enriched in capillary aerocyte (D) and capillary general (E) from IH vs control mice. Enrichment analysis was performed in the DAVID database, using up and down regulated genes (BHQ < 0.2). Redundant biological processes are merged into one category. Top 5 biological processes enriched in up and down regulated genes are indicated in red and blue bars, respectively. The list of endothelial subpopulations include endothelial artery (EndoArt), vein (EndoVein), capillary aerocytes (EndoCap-a), capillary general (EndoCap-g) cells.

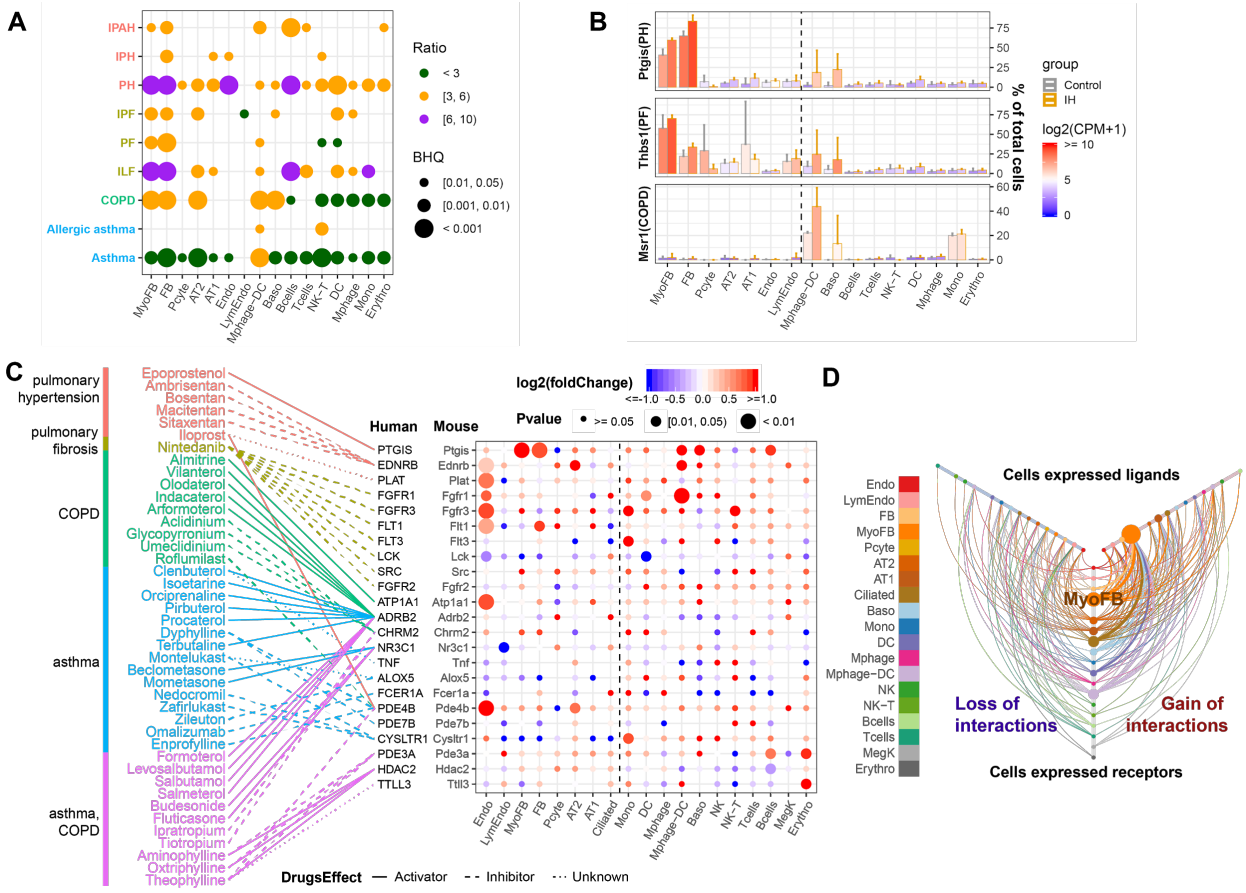

Fig. 6. Pulmonary disease-regulated genes provide clinical implications for OSA at the cell-specific level. (A) Pulmonary disease-associated genes are enriched in up regulated genes in different cell types from whole lungs of mice exposed to IH vs controls. Enrichment analysis was performed in DisGenet human database, using the top 200 up regulated genes identified from each cell type. The enrichment ratio is indicated by color. The point size indicates the enrichment BHQ from a fisher exact test. The pulmonary diseases include asthma, allergic asthma, chronic obstructive airway disease (COPD), interstitial lung fibrosis (ILF), pulmonary fibrosis (PF), idiopathic pulmonary fibrosis (IPF), pulmonary hypertension (PH), idiopathic pulmonary hypertension (IPH), and idiopathic pulmonary arterial hypertension (IPAH). (B) The disease-associated genes vary in expression level and percentage of cells that express those genes. The fold change is indicated by the color, and the percentage of cells that express those genes is indicated by the height of the bar. Control and experimental groups are indicated by grey and orange box borders, respectively. (C) Dozens of pulmonary drug targets show differential expression in multiple cell types in lung from mice exposed to IH. Drug classes used to treat different pulmonary diseases are indicated by text color. Drug effect is indicated by the line type. Fold change is indicated by the point color, and the P-value of differential expression is indicated by the point size. (D) The hive plot shows ligand-receptor interaction changes between pairs of cell types in response to IH. Nodes indicate cell-expressed ligands (horizontal axis) or receptors (vertical axis). Size of nodes are in proportion to the number of interactions changed for the cell type. Width of lines show numbers of interactions gained (right) or lost (left) between the pairs of cell types. The list of cell types include: endothelial cells (Endo), B cells (Bcells), natural killer cells (NK), T cells (Tcells), natural killer cells (NK), natural killer T cells (NK-T), macrophages (Mphage), basophils (Baso), monocytes (Mono), macrophages-dendritic CD163+ cells (Mphage-DC), dendritic cells (DC), megakaryocytes (MegK), fibroblasts (FB), myofibroblasts (MyoFB), pericytes (Pcyte), alveolar type I cells (AT1), lymphatic endothelial cells (LympEndo), erythroblasts (Erythro), alveolar type II cells (AT2), and ciliated cells (Ciliated).

935 **Supplemental figures**

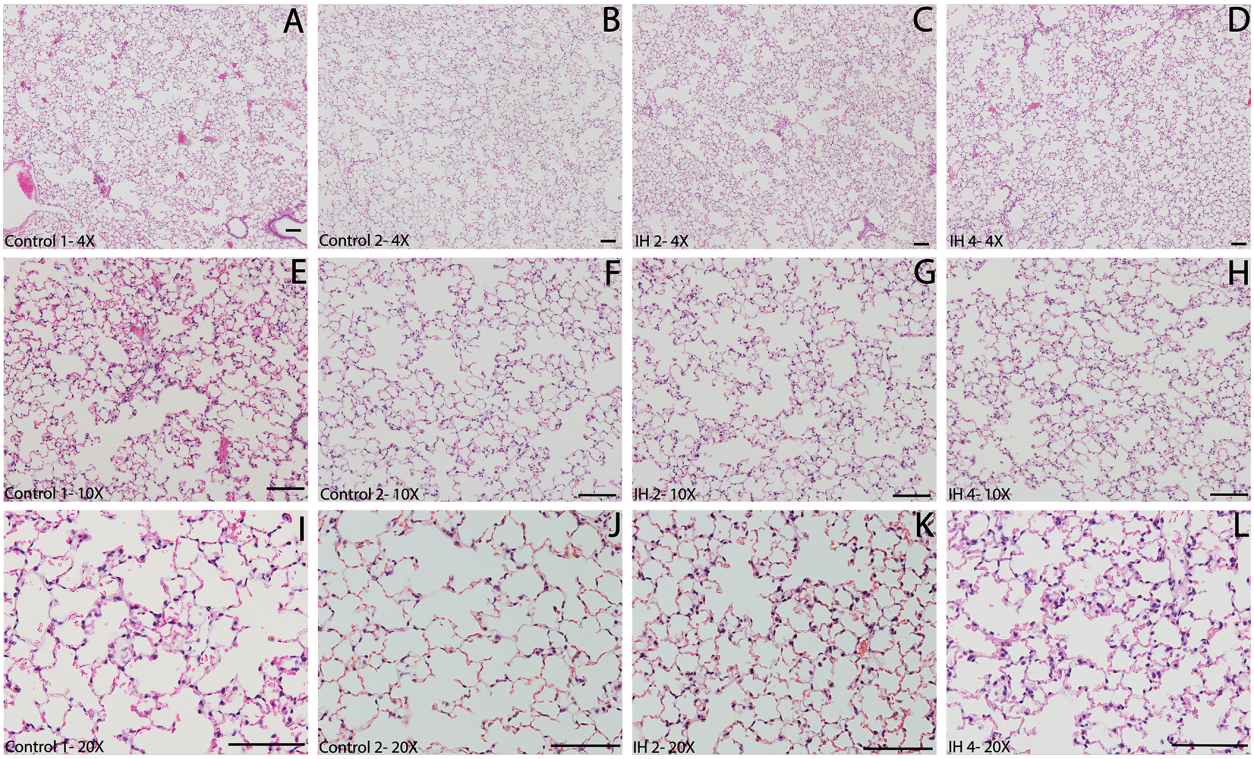

936
937 **Fig. S1. Hematoxylin and eosin–stained sections of whole lung from mice exposed to IH vs**
938 **Controls do not reveal gross histologic changes.** Two representative IH and two control mice with HE
939 stained sections were shown at 4x (A-D), 10x (E-H) and 20x (I-L) magnification. The scale bars all
940 correlate to 100 μm width.

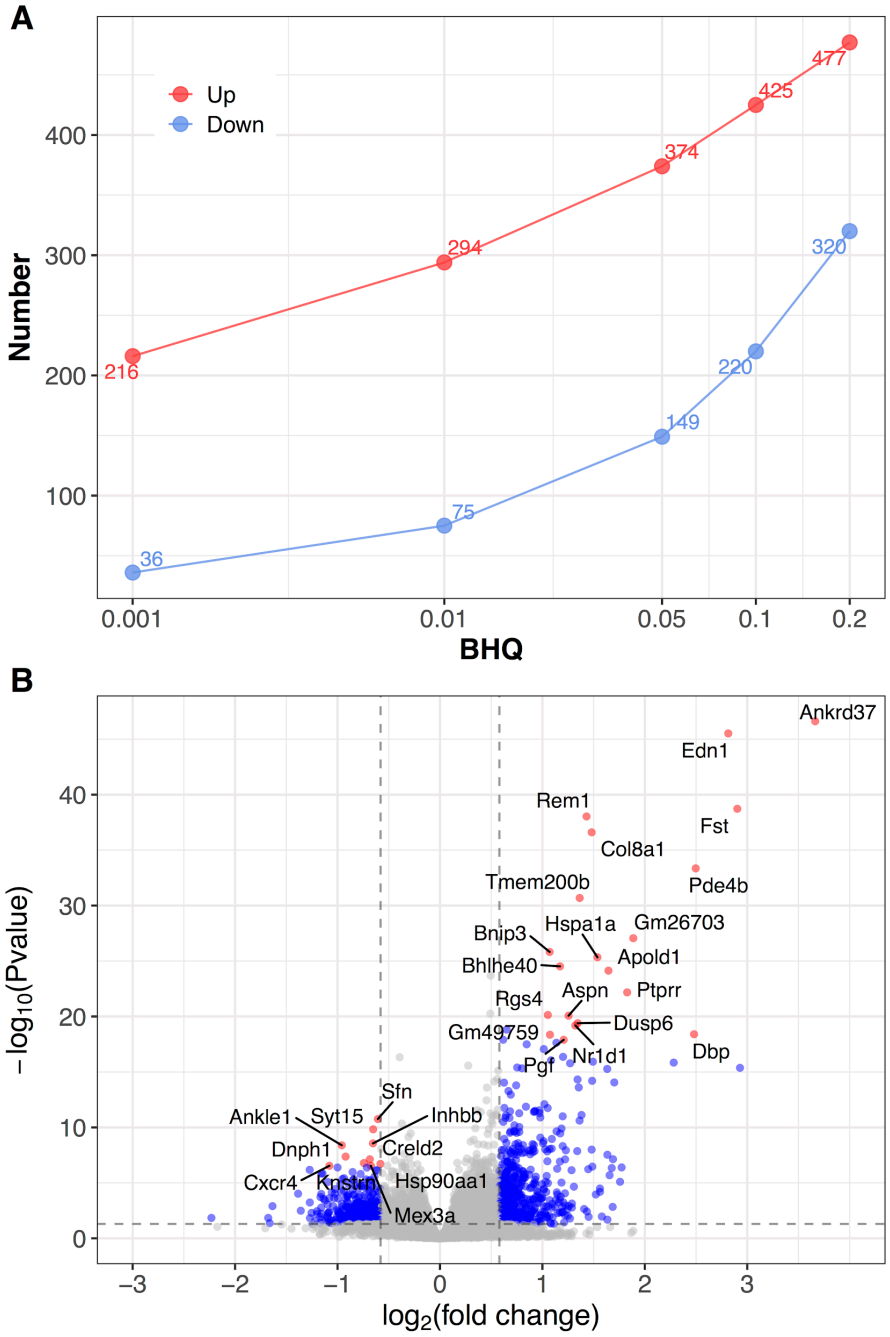

Fig. S2. Differentially expressed genes from bulk RNA-seq analysis of whole lung from mice exposed to IH vs controls. (A) At series BHQ cut-offs, the number of up and down regulated genes in response to IH are shown with red and blue lines, respectively. (B) A volcano plot shows the differentially expressed genes from lung of mice exposed to IH. Ranked by P-value, top 20 up regulated genes and top 10 down regulated genes were labeled.

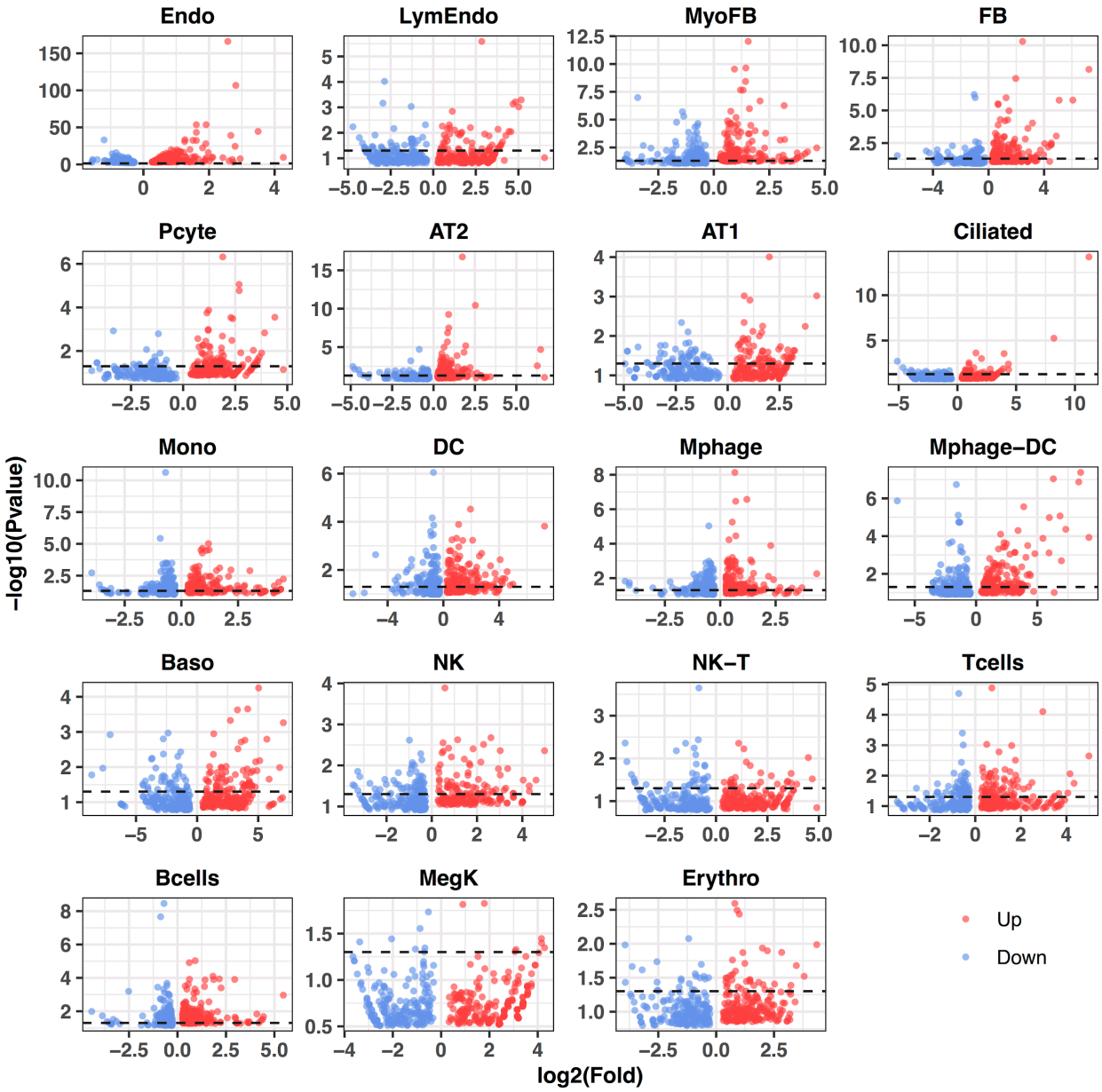

Fig. S3. P-value distribution of the top 200 up and down regulated IH-responsive genes in 19 lung cell types. Each red or blue point indicates one up or down regulated gene. The black dashed line indicates a P-value of 0.05.

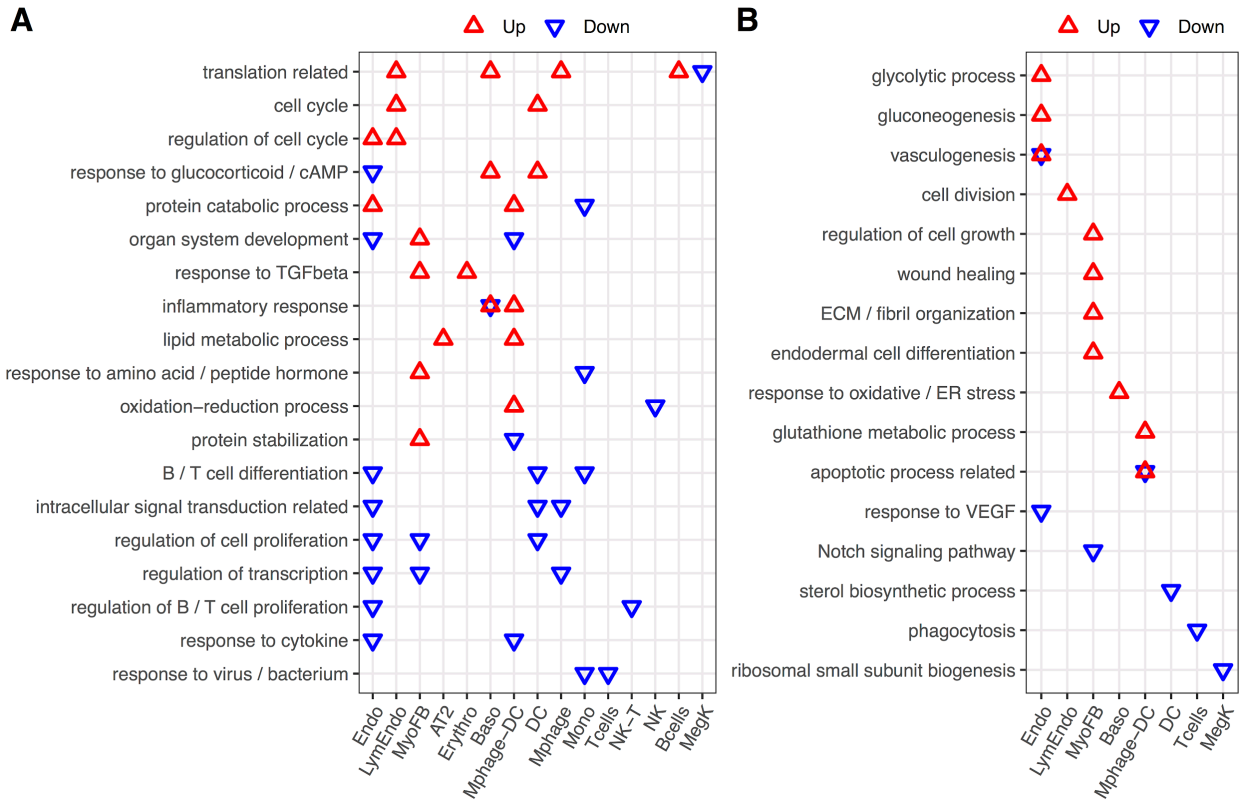

Fig. S4. Enriched biological processes from differentially expressed genes from whole mouse lungs exposed to IH vs controls. Enrichment analysis was performed in the DAVID database using the top 200 up and down regulated genes identified from each cell type. Redundant biological processes are merged into one category. Biological processes enriched in up and down regulated genes are indicated by red and blue triangles, respectively.

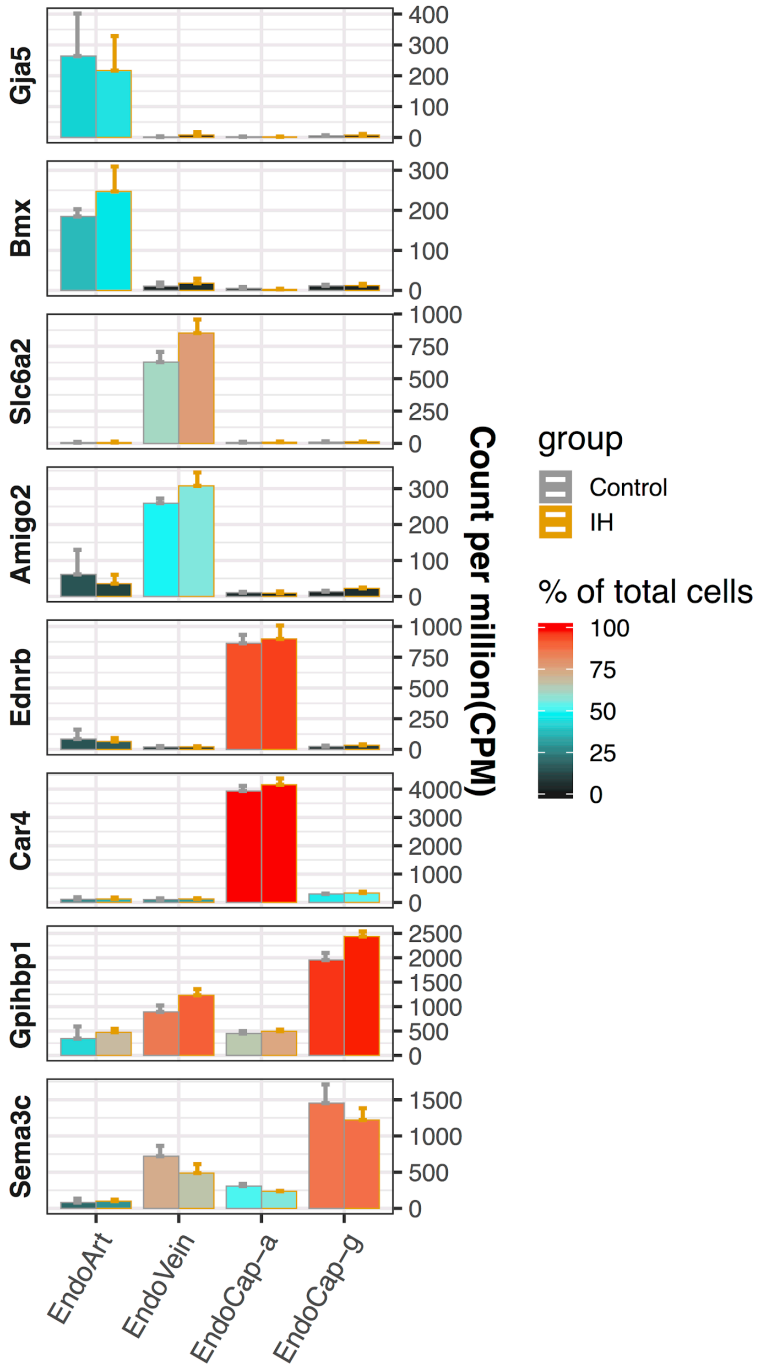

Fig. S5. Validation of endothelial subpopulation assignments with known markers. The marker genes collected from the literature and assigned endothelial subpopulations are listed on the y-axis and x-axis, respectively. The average CPM (count per million reads) of three replicates from control (grey) and IH (orange) mice are indicated by the height of the bar. The error bars indicate standard deviation based on the three biological replicates. The average percentage of cells with detected expression of each marker gene among the endothelial subpopulations is indicated by the heatmap color. The four endothelial subpopulations include endothelial artery (EndoArt), vein (EndoVein), capillary aerocytes (EndoCap-a), and capillary general (EndoCap-g).

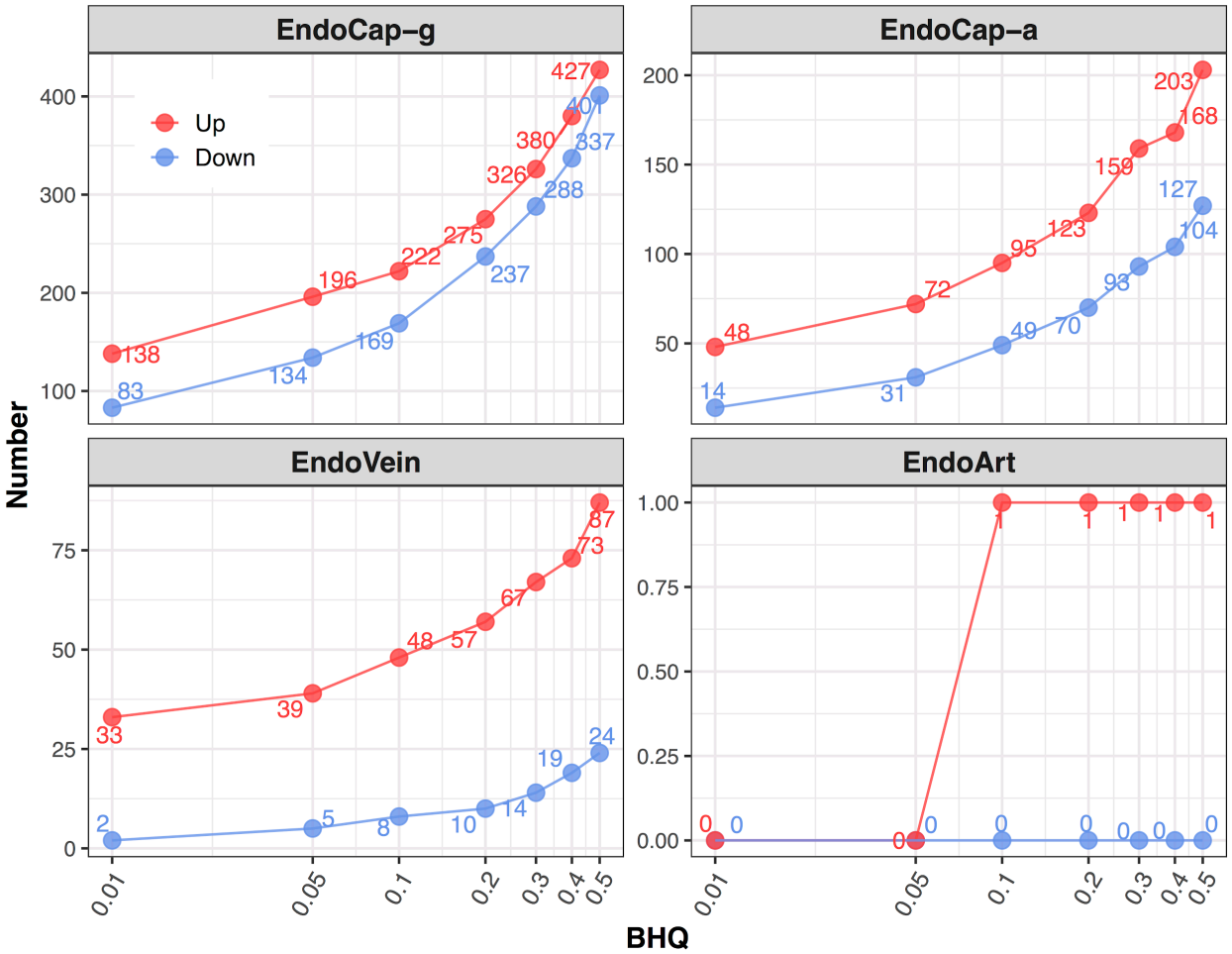

966
967 **Fig. S6. Number of differentially expressed IH-responsive genes in four lung endothelial**
968 **subpopulations using BHQ cut-offs.** At series BHQ cut-offs, the number of up and down regulated
969 genes in lung endothelial subpopulations as a response to IH are shown with red and blue lines,
970 respectively. The four endothelial subpopulations include endothelial artery (EndoArt), vein (EndoVein),
971 capillary aerocytes (EndoCap-a), and capillary general (EndoCap-g).

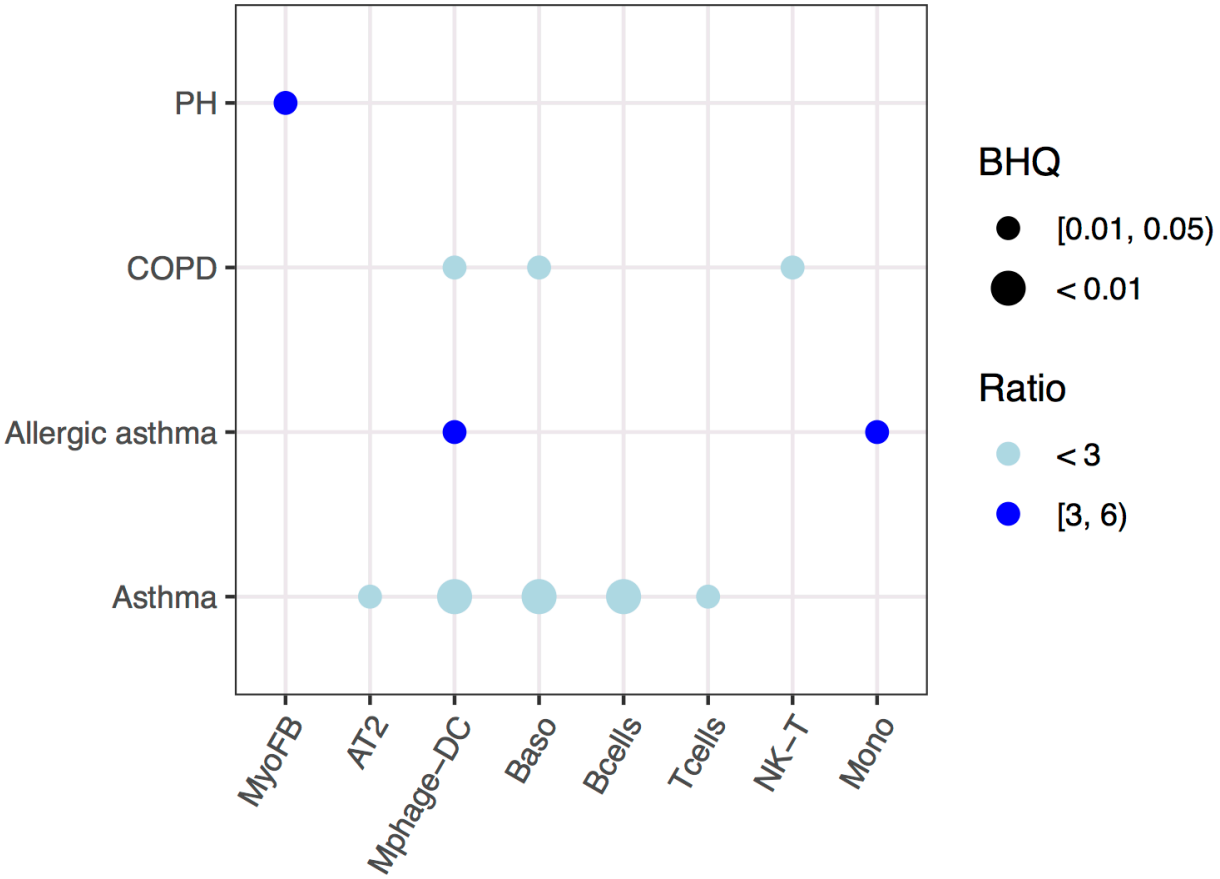

Fig. S7. Pulmonary disease-associated genes are enriched in down regulated genes in different cell types in the lung from mice exposed to IH. Enrichment analysis was performed in the DisGenet database, using the top 200 down regulated genes identified from each cell type. The average fold change of down regulated genes in each cell type for the same disease is indicated by color scale. The point size indicates the enrichment BHQ value from the fisher exact test. The point color indicates the enrichment ratio. The pulmonary diseases include asthma, allergic asthma, chronic obstructive airway disease (COPD), and pulmonary hypertension.

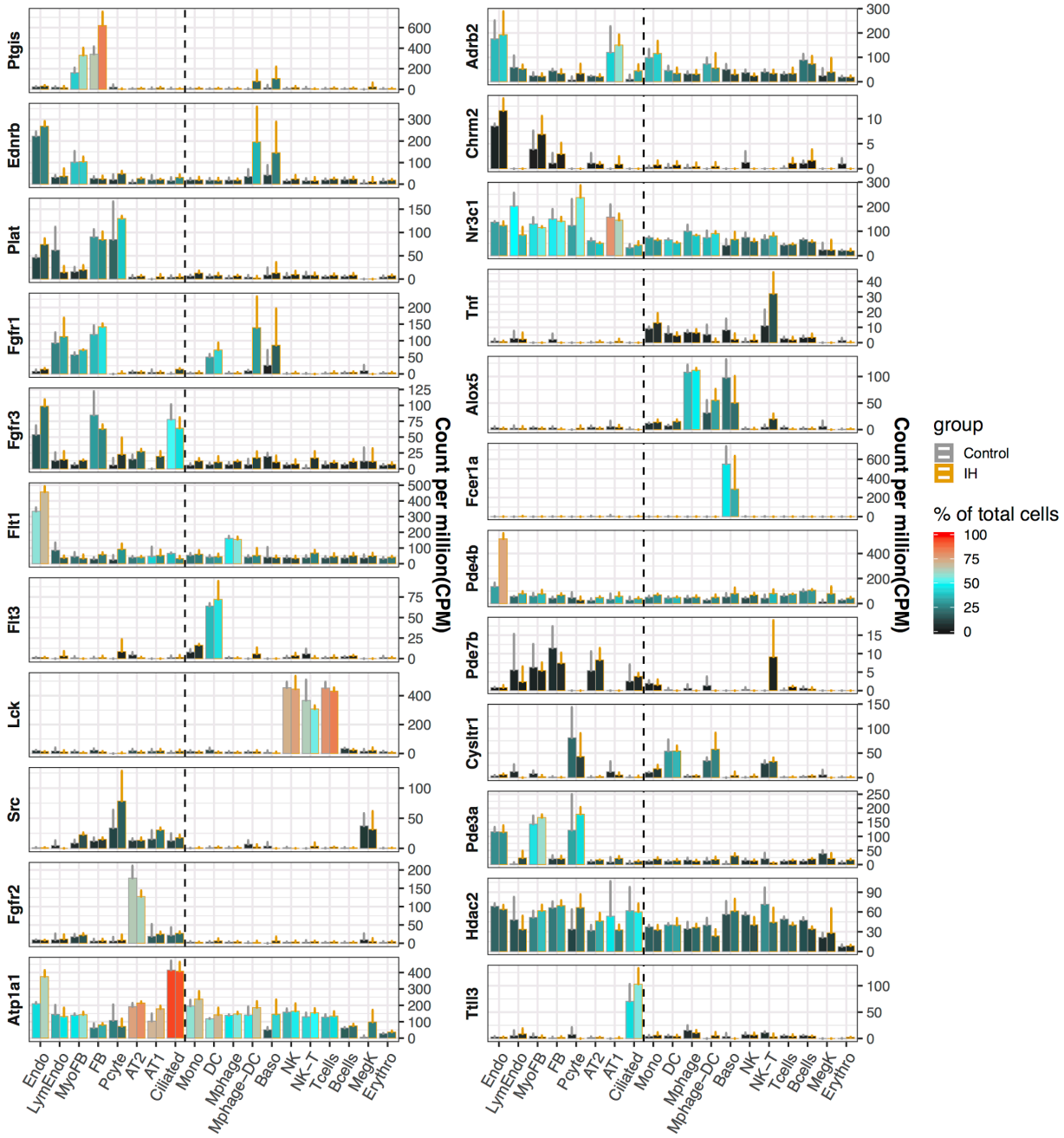

Fig. S8. Pulmonary drug targets with cell type specific expression profiles in mouse lung. The average CPM (count per million reads) of three control (grey) and IH (orange) replicates are indicated by the height of the bar. The error bar indicates standard deviation from the three biological replicates. The average percentage of cells with detected expression of each marker gene among specific cell types is indicated by the color scale. The list of cell types include: endothelial cells (Endo), B cells (Bcells), natural killer cells (NK), T cells (Tcells), natural killer cells (NK), natural killer T cells (NK-T), macrophages (Mphage), basophils (Baso), monocytes (Mono), macrophages-dendritic CD163+ cells (Mphage-DC), dendritic cells (DC), megakaryocytes (MegK), fibroblasts (FB), myofibroblasts (MyoFB), pericytes (Pcyte), alveolar type I cells (AT1), lymphatic endothelial cells (LympEndo), erythroblasts (Erythro), alveolar type II cells (AT2), and ciliated cells (Ciliated).

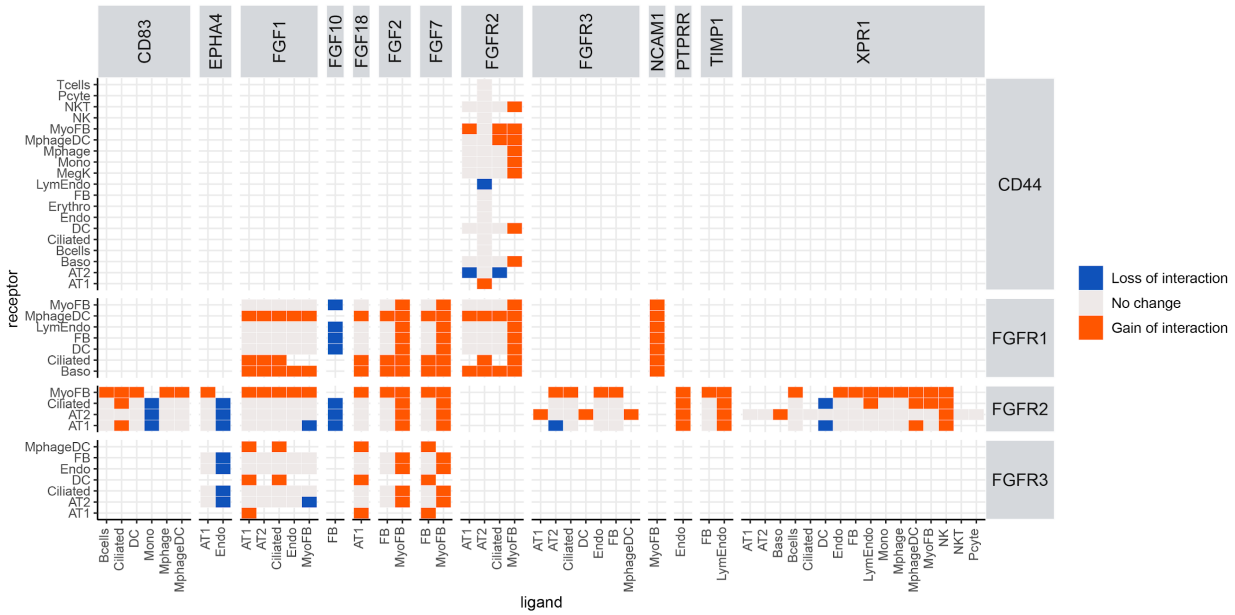

Fig. S9. Ligand-receptor interaction analysis reveals a major role for myofibroblasts in activating the FGF signaling pathway as a response to IH. Heatmap shows ligand-receptor pair interaction changes in different cell pairs. Orange indicates a new interaction found in response to IH but not in control samples (gain of interaction), and blue indicates an interaction found in controls but not in response to IH (loss of interaction). Myofibroblasts show a gain of interaction between FGF2, FGF7 and NCAM1 to the FGF receptor in multiple cell types, indicating its role in activating the FGF signaling pathway in response to IH.

Other Supplementary Material for this manuscript includes the following:

Data file S1 contains the following supplementary tables:

Table S1 (Microsoft Excel format). The alignment statistics of bulk RNA-seq data for IH exposure and control mice.

Table S2 (Microsoft Excel format). Top 200 up and down regulated genes in mice lung under IH exposure from the bulk RNA-seq data.

Table S3 (Microsoft Excel format). DAVID enriched biological processes and merged categories using top 200 differential expression genes from the bulk RNA-seq data.

Data file S2 contains the following supplementary tables:

Table S4 (Microsoft Excel format). The alignment statistics of scRNA-seq data for IH exposure and control mice.

Table S5 (Microsoft Excel format). The marker genes list for 25 clusters from AltAnalyze analysis of scRNA-seq data from IH exposure mice.

Table S6 (Microsoft Excel format). The annotated cell types for 25 cellHarmony aligned clusters of scRNA-seq data from IH exposure and control mice.

Table S7 (Microsoft Excel format). Top 200 up and down regulated genes in 19 detected lung cell types under IH exposure from the scRNA-seq data.

Table S8 (Microsoft Excel format). DAVID enriched biological processes and merged categories using top 200 differential expression genes in each lung cell type under IH exposure.

Data file S3 contains the following supplementary tables:

Table S9 (Microsoft Excel format). The marker genes list for 6 clusters from AltAnalyze analysis of scRNAseq-data from annotated vascular endothelial cells of IH exposure mice.

Table S10 (Microsoft Excel format). The annotated endothelial subpopulations for 6 cellHarmony aligned clusters of scRNA-seq data from annotated vascular endothelial cells of IH exposure and control mice.

1024 Table S11 (Microsoft Excel format). Differential expression genes of 4 annotated endothelial

1025 subpopulations under IH exposure from the scRNA-seq data.

1026 Table S12 (Microsoft Excel format). DAVID enriched biological processes and merged

1027 categories using differential expression genes of lung capillary cells under IH exposure.

1028 **Data file S4 contains the following supplementary tables:**

1029 Table S13 (Microsoft Excel format). The pulmonary disease associated genes from top 200 up

1030 or down regulated genes in each detected lung cell-type exposed to IH.